Research Square

Preprints are preliminary reports that have not undergone peer review.
They should not be considered conclusive, used to inform clinical practice,
or referenced by the media as validated information.

Microglial NEDD4L activates mtDNA-cGAS-STING pathway and promotes neuroinflammation after intracerebral hemorrhage through impairing mitophagy

Jin Wang
Zhejiang Provincial People's Hospital, Hangzhou Medical College
Yuyuan Ma
Zhejiang Provincial People's Hospital, Hangzhou Medical College
Kaichuang Yang
Zhejiang Provincial People's Hospital, Hangzhou Medical College
Weihua Zhang
Zhejiang Provincial People's Hospital, Hangzhou Medical College
Weiyu Wang
Zhejiang Provincial People's Hospital, Hangzhou Medical College
Yuhao Zhang
Zhejiang Provincial People's Hospital, Hangzhou Medical College
Shucai Fan
Zhejiang Provincial People's Hospital, Hangzhou Medical College
Shenglian Wu
Zhejiang Provincial People's Hospital, Hangzhou Medical College
Xin Gao
Zhejiang Provincial People's Hospital, Hangzhou Medical College
Shenghao Zhang
the First Affiliated Hospital of Xi'an Jiao Tong University
Xun Wu
Tangdu Hospital, the Fourth Military Medical University
Bing Lei
zjsrmyysjwk@163.com

Zhejiang Provincial People's Hospital, Hangzhou Medical College

Research Article

Keywords: brain injury, microglia, neuroinflammation, NEDD4L, cGAS-Sting, mitophagy

Posted Date: April 6th, 2026

DOI: https://doi.org/10.21203/rs.3.rs-9225741/v1

License: This work is licensed under a Creative Commons Attribution 4.0 International License.
Read Full License

Additional Declarations: No competing interests reported.

Microglial NEDD4L activates mtDNA-cGAS-STING pathway and promotes neuroinflammation after intracerebral hemorrhage through impairing mitophagy

Jin Wang[1,#], Yuyuan Ma[1,#], Kaichuang Yang[1,#], Weihua Zhang[1], Weiyu Wang[1], Yuhao Zhang[1], Shucai Fan[1], Shenglian Wu[1], Xin Gao[1], Shenghao Zhang[3], Xun Wu[2,*], Bing Lei[1,*]

1 Department of Neurosurgery, Zhejiang Provincial People's Hospital, Hangzhou Medical College, Hangzhou, 310000, Zhejiang, China.

2 Department of Neurosurgery, Tangdu Hospital, the Fourth Military Medical University, Xi'an 710032, Shaanxi, China

3 Department of Neurosurgery, the First Affiliated Hospital of Xi'an Jiao Tong University, Xi'an 710032, Shaanxi, China

[#] These authors contributed equally to this work.

*Corresponding author:

Bing Lei, Zhejiang Provincial People's Hospital, Hangzhou Medical College, Hangzhou, 310000, Zhejiang, China. E-mail addresses: zjsrmyysjwk@163.com.

Xun Wu, Tangdu Hospital, the Fourth Military Medical University, Xi'an 710032, Shaanxi, China. E-mail addresses: 2645302700@qq.com.

Abstract

Background: The resultant microglial activation and sustained neuroinflammatory response are key contributors to secondary injury, promoting blood-brain barrier disruption, cerebral edema, and progressive neuronal loss. Although NEDD4L has been implicated in inflammation and immunity, the functions of NEDD4L in acute brain injury and microglia-specific responses remain largely unknown in intracerebral hemorrhage(ICH).

Methods: Using proteomic sequencing, single-cell RNA sequencing, Immunofluorescence Staining. flow cytometry analysis, we investigated cellular distribution and expression of NEDD4L in ICH. Genetically engineered mouse models, neurological function testing, flow cytometry analysis, engineering extracellular vesicle (EV) isolation and TUNEL staining, we investigated the role of NEDD4L in ICH. Protein interactions was used for mechanism analysis.

Results: We identified a substantial upregulation of the ubiquitin ligase NEDD4L in isolated microglia following ICH, and demonstrated that its increase is mediated by STAT2-dependent transcriptional mechanisms. Microglial subpopulations with high NEDD4L expression exhibit a pronounced pro-inflammatory phenotype. Moreover, knockout of NEDD4L specifically in microglia conferred neuroprotection and attenuated innate immune responses by the cytosolic DNA-sensing pathway. Mechanistically, NEDD4L promotes the ubiquitination of Parkin, resulting in the leakage of mitochondrial DNA into the cytoplasm and subsequent activation of the cGAS–Sting inflammatory cascade. Engineered extracellular vesicles of NEDD4L-specific siRNA successfully mitigated neuroinflammation, tissue damage, and functional deficits—in both ICH and TBI mouse models.

Conclusions: we unveil a novel role for NEDD4L in modulating microglia-driven neuroinflammation after acute brain injury and highlight its function in activating the

mtDNA–cGAS–Sting signaling axis.

Keywords: brain injury; microglia; neuroinflammation; NEDD4L; cGAS-Sting; mitophagy

INTRODUCTION

As the principal immune guardians of the central nervous system (CNS), microglia maintain neural homeostasis through constant parenchymal surveillance and execution of essential functions, including synaptic refinement, clearance of cellular debris, and secretion of trophic factors[1-3]. While these activities are protective under physiological conditions, dysregulated microglial responses after acute CNS injuries—such as intracerebral hemorrhage (ICH) and traumatic brain injury (TBI)—can exacerbate pathology[4-7]. Following acute brain injury, extensive neuronal necrosis releases abundant damage-associated molecular patterns (DAMPs), which function as potent alarm signals that drive microglial phenotypic transformation. The resultant microglial activation and sustained neuroinflammatory response are key contributors to secondary injury, promoting blood-brain barrier disruption, cerebral edema, and progressive neuronal loss[8-10]. Therefore, identifying molecular regulators that govern microglial polarization after acute brain injury represents a critical research priority.

NEDD4L, a HECT-type E3 ubiquitin ligase in the NEDD4 family, modulates multiple biological processes including TGF-β signaling, and mitochondrial homeostasis[11-13]. Its role in inflammation is context-dependent: NEDD4L enhances antiviral immunity by facilitating K29-linked ubiquitination of TRAF3 and TBK1–IRF3–driven interferon production, yet it also promotes pro-inflammatory M1 macrophage polarization and NF-κ

B signaling[14, 15]. In neurological diseases, NEDD4L exhibits divergent effects. It is downregulated in Alzheimer's disease, suggesting a loss of neuroprotective regulation, whereas in Huntington's disease, it impairs mitochondrial metabolism by degrading LIPT2[12, 16]. Nevertheless, the functions of NEDD4L in acute brain injury and microglia-specific responses remain largely unknown.

The cytosolic DNA sensor cyclic GMP-AMP synthase (cGAS) functions as the primary innate immune sentinel responsible for detecting aberrant double-stranded DNA (dsDNA) within the cell cytoplasm[17-19]. Upon binding to dsDNA fragments, which can originate from various sources including invading pathogens, genomic instability, or damaged organelles, cGAS undergoes a conformational shift that activates its enzymatic function. This activation catalyzes the synthesis of the critical second messenger molecule, cyclic guanosine monophosphate–adenosine monophosphate (2'3'-cGAMP). This newly formed cGAMP molecule then acts as a high-affinity ligand, binding directly to and activating the endoplasmic reticulum (ER)-resident adapter protein Sting(Stimulator of Interferon Genes). Sting serves as an indispensable central hub in the innate immune system's interferon response cascade, initiating broad antiviral and inflammatory programs[20-22]. Mounting evidence implicates the dysregulation or chronic activation of this cGAS- Sting signaling axis in the pathogenesis of diverse central nervous system (CNS) disorders, contributing to brain injuries[23-26]. Despite its established role in these related neurological pathologies, the specific contributions, temporal dynamics, and cell-type specificity of the cGAS- Sting pathway in the context of avute brain injury remain predominantly undefined and represent a significant gap in potential immunomodulatory therapeutic targets.

In this study, we investigated the molecular mechanisms driving pathogenic gene expression in microglia after acute insult. We found that STAT2-mediated transcriptional

upregulation enhances NEDD4L expression in microglia post-injury. Functionally, NEDD4L promotes inflammation by suppressing Parkin-dependent mitophagy, leading to mtDNA leakage and activation of the cGAS–Sting pathway. Importantly, microglia-targeted knockdown of NEDD4L via engineered extracellular vesicles loaded with siRNA attenuated neuroinflammation, brain edema, neuronal death, and neurological deficits in both ICH and TBI models. These results identify NEDD4L as a key mediator of microglial dysfunction and suggest a potential therapeutic strategy for neuroinflammatory CNS conditions.

MATERIALS AND METHODS

Experimental Animals

Male C57BL/6J mice (8–12 weeks old) were sourced from the Animal Center of Zhejiang Provincial People's Hospital. To induce microglia-specific deficiency of NEDD4L in mice, we first mating NEDD4L$^{flox/flox}$ mice with Tmem119-CreERT animals (both from Shanghai Model Organisms Center) to generate NEDD4L$^{flox/flox}$: Tmem119-CreERT+ mice. Tamoxifen (Selleck, #S1238; 200 mg/kg) was administered intraperitoneally once daily for five consecutive days to induce recombination. Control groups consisted of NEDD4Lflox/flox littermates treated with tamoxifen but lacking Cre expression. All experiments were initiated after a 14-day washout period. Mice were housed under controlled environmental conditions (22 ± 1 °C) with unrestricted access to food and water. All experimental protocols received approval from the Animal Eth-ics Committee of Zhejiang Provincial People's Hospital.

Intracerebral Hemorrhage Model

Animals were deeply anesthetized with 2% pentobarbital sodium administered intraperitoneally and then immobilized in a stereotaxic frame. ICH was induced by stereotaxically injecting bacterial collagenase VII-S (Sigma-Aldrich, C2399; 0.075 U in 0.2 μl saline) into the right striatum[27]. Following scalp sterilization and a midline incision, a burr hole (diameter 0.5 mm) was created at the following coordinates relative to bregma: 0.20 mm anterior, 2.30 mm lateral. Collagenase was infused at 0.05 μl/min to a depth of 3.20 mm below the dura. The injection needle was retained in place for 5 minutes post-infusion to minimize reflux. Sham-operated animals underwent the same surgical steps without collagenase injection.

Traumatic Brain Injury Model

A controlled cortical impact (CCI) model was utilized to induce TBI[28]. The surgical procedure began with anesthetizing and stereotaxically stabilizing the mouse. Subsequently, a 3-mm cranial window was drilled at a site 1.5 mm posterior and lateral to bregma. Impact was delivered perpendicularly to the exposed cortex using a 2-mm piston tip, which was advanced at 3 m/s to a depth of 1.5 mm for a dwell time of 200 ms. The sham group underwent craniotomy without the subsequent cortical impact.

Immunofluorescence Staining

After euthanasia via pentobarbital sodium overdose, mice were transcardially perfused with chilled PBS followed by 4% paraformaldehyde (PFA). Brain samples were post-fixed in 4% PFA for 6 hours at 4°C and then cryoprotected using a graded sucrose series (10%, 20%, 30%). Coronal sections (15 μm thick) were permeabilized with 0.1% Triton X-100

for 30 minutes and blocked with 10% donkey serum for 2 hours. Sections were incubated with primary antibodies overnight at 4°C, followed by appropriate fluorescent secondary antibodies. Antibodies used were: NEDD4L (Proteintech, 13690-1-AP), Iba1 (Abcam, ab289874), and CD68 (Abcam, ab283654).

Microglia isolation

Microglia were extracted following a modified version of the method by Glass et al[29]. Briefly, brain tissue was gently dissociated mechanically, and microglial purification was achieved via Percoll density gradient centrifugation. After multiple PBS washes, cells were labeled with fluorescent antibodies and sorted as CD11b+CD45Low single cells on a BD Influx sorter.

Western Blots

Protein lysates were prepared using RIPA buffer containing protease inhibitors and quantified via BCA assay (Thermo Scientific). Proteins were separated by SDS-PAGE and transferred to PVDF membranes. Membranes were blocked with 5% non-fat milk and probed overnight at 4°C with primary antibodies. Following TBST washes, HRP-conjugated secondary antibodies were applied for 2 hours at room temperature. Protein bands were visualized using chemiluminescence (BioRad). Primary antibodies included: NEDD4L (Proteintech, 13690-1-AP), cGAS (Novus, NBP3-16666), Sting (Cell Signaling Technology, D2P2F), TBK1 (Cell Signaling Technology, D1B4), phospho-TBK1 (Cell Signaling Technology, D52C2), Parkin (Proteintech, 14060-1-AP), TIM50 (Cell Signaling Technology, #62317), TOM20 (Cell Signaling Technology, D8T4N), LC3(Cell Signaling Technology, #12741), and β-actin (Proteintech, 2D4H5).

Co-immunoprecipitation (Co-IP)

Cell lysates prepared in IP buffer (Thermo Scientific) with protease inhibitors were rotated at 4°C for 4 hours and centrifuged at 10,000 × g for 10 minutes. Supernatants (1 mg protein) were incubated with 2 μg of the relevant antibody overnight at 4°C. Antibodies used for IP were anti-Ubiquitin (Santa Cruz, sc-8017), anti-NEDD4L (Proteintech, 13690-1-AP), and anti-Parkin (Proteintech, 14060-1-AP). Protein A/G magnetic beads (MCE) were then introduced and incubated for 4 hours. Beads were washed three times with IP buffer, and immunoprecipitated proteins were eluted using Laemmli buffer.

TUNEL staining

Apoptotic cells were labeled using a TUNEL detection kit (Roche) per the manufacturer's instructions. Tissue sections were treated with 0.3% hydrogen peroxide for 30 minutes and then digested with 0.25% proteinase K at 37°C for 45 minutes. After incubation with the TUNEL reaction mixture in the dark for 1 hour at 37°C, nuclei were counterstained with DAPI. The proportion of TUNEL-positive cells relative to total DAPI-stained nuclei was used to quantify apoptosis. Evaluation was performed in a blinded manner, with data derived from at least three independent experiments.

Chromatin immunoprecipitation (ChIP)-qPCR

ChIP assays were conducted using a commercial kit (Cell Signaling Technology, #9003). Cells were cross-linked with 1% formaldehyde for 10 minutes at room temperature, and

the reaction was quenched with glycine. After PBS washes, chromatin was fragmented by sonication in ChIP buffer. Sheared chromatin (50–200 μg/mL DNA) was immunoprecipitated overnight at 4°C with an anti-FLAG antibody (Proteintech, 20543-1-AP) or control IgG. Protein G magnetic beads were added for 2 hours, and bound chromatin was eluted and reverse cross-linked. Purified DNA was analyzed by qPCR.

Luciferase reporter assay

Cells were seeded in 24-well plates (1×10^5 cells/well). The NEDD4L promoter (wild-type or mutant) was inserted into the pGL3-basic vector (Genecreate). Constructs were cotransfected with or without an STAT2 overexpression plasmid. After 48 hours, luciferase activity was quantified using a dual-luciferase reporter system (Promega). Firefly luciferase values were normalized to Renilla luciferase activity.

Neurological function testing

Rotarod Test: Motor coordination and balance were evaluated using an accelerating rotarod. Each animal was placed on the rod, which was progressively accelerated from 4 to 40 rpm over a 5-minute period. The latency to fall was recorded. Every mouse completed three consecutive trials with 5-minute inter-trial rests, and the average latency from these trials was used for analysis.

Adhesive Removal Test: Somatosensory function was evaluated by applying a small adhesive patch (2x3 mm) to the plantar surface of the left forepaw. The time for the mouse to first sense and initiate contact with the tape (latency to contact) and the total

time to completely remove it (removal time) were recorded. A cut-off time of 120 seconds was set per trial.

Grid-Walking Assay: Spontaneous locomotor coordination was assessed via a grid-walking task. Mice were allowed to freely ambulate on an elevated wire grid for one minute while being video-recorded. A foot fault was counted each time a paw slipped through the grid opening. The total number of steps and faults were quantified, and the fault rate was expressed as the percentage of faulty steps relative to the total steps taken.

Brain Water Quantification

Brains were quickly removed and was weighed immediately (wet weight) and again after 48 hours of drying at 95–100°C (dry weight). The water content percentage was determined as: [(wet weight − dry weight) / wet weight] × 100%.

Flow cytometry analysis

Brains were harvested into cold HBSS and dissociated enzymatically using Papain (2 mg/ml, Worthington 3119) for 60 minutes at 37°C. Cell suspensions were filtered (70 μm) and myelin was removed by centrifugation (900 g, 25°C, 25 min) through a 30% Percoll gradient (GE Healthcare 17-0891-09). Pelleted cells were collected, washed, and resuspended in PBS containing 2% FBS. Surface staining utilized: APC-eFluor780 anti-CD45 (Thermo 47-0451-82), PE anti-Ly6G (Thermo 16-9668-82), Pacific Blue anti-Ly6C (BioLegend 128064), and PE-Cy7 anti-CD3e (Thermo 25-0031-82). After 60-minute antibody incubation, cells were washed and analyzed on a NovoCyte flow cytometer using NovoExpress software.

Primary Microglial Culture

Microglia were obtained from postnatal day 1–3 C57BL/6J pups. After meninges removal, brain tissue was digested with 0.25% trypsin, filtered, and plated in poly-D-lysine–coated flasks with DMEM GlutaMAX containing 10% FBS and 1% penicillin/streptomycin. After 7 days, microglia were detached by shaking (200 rpm, 1 hour) and expanded for 7 days with M-CSF (20 ng/ml).

Extracellular vesicle (EV) isolation and engineering

HEK293T cells were maintained under standard culture conditions (5% CO_2) in Dulbecco's modified Eagle's medium (DMEM, Corning) containing dialyzed fetal bovine serum (Gibco) and antibiotics (hygromycin B from Roche and puromycin from GPC Biotechnology). To isolate EVs, the conditioned medium was first spun at 300 × g for 5 minutes to pellet cellular material. Subsequent centrifugation steps included 10,000 × g for 60 minutes to eliminate large vesicles and 3,000 × g for 30 minutes to clear debris. The clarified supernatant was passed through a 0.22 μm filter and ultracentrifuged at 200,000 × g for 90 minutes. The resulting pellet was washed and purified further via resuspension in PBS and another round of ultracentrifugation under the same conditions.

Fabrication of cRGD-Modified EVs

Engineered cRGD-EVs were generated using a lipid fusion and extrusion approach based

on previously established protocols[30]. Briefly, a mixture of cholesterol, lecithin, and DSPE-PEG-cRGD at a weight ratio of 4:2:1 was dissolved in 2 mL of tetrahydrofuran (THF) under sonication (50 kHz, 30 minutes). The organic solvent was evaporated using a rotary evaporator at 50 °C for 1 hour. The resulting lipid film was rehydrated in 1 mL PBS to form cRGD-functionalized liposomes. These liposomes were co-incubated with isolated EVs at 37 °C for 15 minutes and then extruded repeatedly through a 200 nm polycarbonate membrane using a Mini extruder (Avanti Polar Lipids) to produce cRGD-EVs.

Characterization of Isolated Vesicles

Purified EVs were characterized using multiple techniques[31]. Western blot analysis was conducted with antibodies against classic EV markers: CD63 (25682-1-AP, Proteintech), CD9 (20597-1-AP, Proteintech), and TSG101 (14497-1-AP, Proteintech). Morphological assessment was performed via transmission electron microscopy (TEM). Samples were adsorbed onto formvar-carbon copper grids, stained with 2% uranyl acetate, and imaged at 80 kV. Size distribution was evaluated using dynamic light scattering (Nano ZS-90, Malvern).

In Vivo Tracking of EV Biodistribution

To assess organ distribution in vivo, 200 μg of DiR-labeled EVs and cRGD-EVs were injected intravenously into mice. After 24 hours, fluorescence was captured with an IVIS imaging system (Xenogen) using 620 nm excitation and 670 nm emission filters to visualize and quantify biodistribution.

Statistical Analysis

Data were analyzed using GraphPad Prism 8.0 and are expressed as mean ± SD. Group comparisons employed unpaired t-tests (two groups), one-way ANOVA with Tukey's test (≥3 groups), or two-way ANOVA with Bonferroni correction (multiple groups). Sample sizes were determined by power analysis. Researchers were blinded to group assignments during experiments and analysis. A p-value < 0.05 was considered statistically significant.

RESULTS

STAT2-Mediated NEDD4L Upregulation in inflammatory Microglia

Genes must undergo transcription into mRNA and subsequent translation into proteins to execute their biological functions. To investigate microglial protein dysregulation following ICH, we conducted proteomic sequencing on microglia isolated from ICH mouse model brains. This approach identified 432 significantly upregulated and 725 downregulated proteins（Figure 1A）. Pathway enrichment analysis revealed a pronounced engagement of inflammatory cascades. Specifically, Gene Ontology (GO) terms related to innate immune response were markedly enriched（Figure S1A）. Kyoto Encyclopedia of Genes and Genomes (KEGG) pathway analysis further indicated activation of multiple inflammatory pathways, including the NOD-like receptor and NF-κB signaling pathways—all consistent with the well-established role of microglia as central neuroinflammatory mediators after ICH(Figure S1B).

Among the significantly dysregulated E3 ubiquitin ligases detected in microglia post-ICH, we prioritized NEDD4L for further investigation due to its documented

immunoregulatory functions and unexplored role in microglial pathophysiology（Figure 1B）. Immunoblotting confirmed elevated NEDD4L protein levels in ICH-derived microglia(Figure 1C-D). This upregulation was further corroborated by immunofluorescence staining, which showed clear co-localization of NEDD4L with the microglial marker Iba1（Figure 1E）.

Additionally, we validated NEDD4L alterations in microglia using single-cell RNA sequencing data from patients with acute brain injuries, including ICH and TBI(Figure 1F) [32]. Compared with control samples, NEDD4L mRNA levels were significantly elevated in microglia from both ICH and TBI patients(Figure 1G). To determine whether NEDD4L upregulation occurs uniformly across all microglia or is restricted to specific subtypes, we further identified several distinct microglial subclusters(Figure 1H)and observed that NEDD4L was specifically highly expressed in cluster 3 microglia (Figure 1I). This cluster exhibited significant expansion following ICH or TBI (Figure 1J). Moreover, cluster 3 microglia were characterized by enrichment in proinflammatory(Figure 1K) and neurotoxic pathways associated with pathogenic microglial activities in ICH and TBI, including inflammatory response, chemokine production, and NF-κB signaling pathway activation (Figure L-M). Thus, human evidence supports our findings that NEDD4L is markedly upregulated in microglia after ICH or TBI and is closely associated with inflammatory responses.

The result of qPCR analysis indicates that the NEDD4L mRNA expresion is markedly upregulated in microglia after ICH(Figure 1N). Correspondingly, in vitro studies using primary mouse microglia stimulated with LPS also showed substantial induction of NEDD4L(Figure S1C-E). Together, these findings establish NEDD4L as an inflammation-associated protein upregulated during microglial activation following acute brain injury.

Investigation into the regulatory mechanisms revealed progressive increases in NEDD4L mRNA levels both in vivo after ICH and in LPS-treated primary microglia, suggesting transcriptional regulation. We therefore hypothesized that NEDD4L upregulation might result from altered activity of upstream transcription factors. JASPAR database analysis nominated Stat2 as a high-scoring candidate, which was further supported by its upregulated expression in our proteomic dataset(Figure 1O). Chromatin immunoprecipitation coupled with quantitative PCR (ChIP-qPCR) confirmed STAT2 binding to the NEDD4L promoter(Figure 1P). Direct transcriptional activation was demonstrated by Stat2-dependent enhancement of NEDD4L promoter activity in dual-luciferase reporter assays(Figure 1Q). Importantly, Stat2 knockdown substantially attenuated NEDD4L expression in LPS-stimulated primary microglia by qPCR (Figure 1R) nd Immunoblotting analysis(Figure 1S-T). These data collectively establish Stat2 as a key transcriptional driver of NEDD4L upregulation in inflammatory microglia.

Conditional Microglial NEDD4L Ablation Improved Functional Outcomes After ICH

To investigate microglial NEDD4L's contribution to secondary injury following ICH, we generated conditional knockout mice ($NEDD4L^{CKO}$) by crossing NEDD4L-floxed mice with TMEM119-creERT2 mice, followed by tamoxifen induction. Volumetric analysis of lesion size further indicated diminished parenchymal damage in mice lacking microglial NEDD4L(Figure 2B-C). Consistent with this neuroprotection, brain water content measurements demonstrated reduced edema formation in knockout animals(Figure 2D). Nissl staining further confirmed increased neuronal survival in $NEDD4L^{CKO}$ mice at 3 days after ICH(Figure 2E-F). Quantitative TUNEL assays revealed significantly attenuated neuronal apoptosis in $NEDD4L^{CKO}$ mice compared to $NEDD4L^{fl/fl}$ controls at equivalent post-ICH timepoints(Figure 2G-H). Furthermore, comprehensive behavioral assessments revealed functional deterioration in knockout mice. Sensorimotor function was evaluated

through adhesive removal tests, grid-walking test, cylinder test and rotarod test. In adhesive removal test, ICH-impaired mice showed prolonged tape removal times, with NEDD4L^{CKO} mice exhibiting significantly attenuated deficits(Figure 2I). As for rotarod performance, the mean fall latency decreased substantially post-ICH, with was mitigated in knockout cohorts(Figure 2L). Similar results were observed in grid-walking test(Figure 2J) and cylinder test(Figure 2K). Collectively, these findings suggest that the ablation of microglial NEDD4L improved neurological outcomes following ICH.

Microglial NEDD4L Depletion Attenuates Local Glial Activation and Peripheral Immune Infiltration Post-ICH

As the innate immune cells of the CNS, microglia are key players in neuroinflammation, responding to damage by releasing cytotoxic factors and regulating peripheral immune cell influx. First, we quantified microglial activation dynamics through density and morphological assessments. NEDD4L^{CKO} ICH mice demonstrated substantially fewer CD68+microglia - a key activation marker - versus NEDD4L$^{flox/flox}$ controls(Figure 3A-C). Fractal dimension analysis revealed ICH-induced microglial transformation toward an amoeboid, hyper-ramified morphology characteristic of reactivity(Figure 3D). These activation-associated structural changes were significantly mitigated in NEDD4L-deficient microglia(Figure 3E-H). Meanwhile, conditional knockout markedly suppressed M1-associated gene expression while enhancing M2 markers following ICH, indicating impaired pro-inflammatory phenotype acquisition(Figure S2A-C). Inflammatory microglia exhibit neurotoxic properties. Moreover， transcriptomic profiling of brain tissues influenced by NEDD4L expression revealed a substantial dysregulation of gene activity in NEDD4L^{CKO} ICH mice compared to NEDD4L$^{fl/fl}$ ICH mice. Specifically, 1118 genes were significantly downregulated and 11 were upregulated in the absence of functional NEDD4L（Figure S2D）. Functional

enrichment analyses, including KEGG and GO, demonstrated that the downregulated genes were strongly associated with inflammatory cascades and immune response pathways, aligning with the previously established role of NEDD4L in modulating microglial inflammatory processes(Figure S2E-F). As expected, primary neurons were exposed to conditioned media from LPS-stimulated microglia(Figure I). Control media induced significant neuronal death, whereas media from NEDD4L-knockdown microglia substantially preserved neuronal viability(FigureJ-K). Meanwhile, we quantified CNS infiltration of peripheral immune cells. As is shown in Figure L-P, flow cytometry analysis demonstrated comprehensive reduction in brain-infiltrating leukocytes including neutrophils ($CD45^{high}Ly6G^{+}$, macrophages/monocytes ($CD45^{high}$Ly6G-Ly6C), $CD4^{+}$T cells ($CD45^{high}CD3e^{+}CD4^{+}$), and $CD8^{+}$T cells ($CD45^{high}CD3e^{+}CD8^{+}$) in $NEDD4L^{CKO}$ mice. Consequently, NEDD4L emerges as a pivotal upstream regulator governing the neurotoxic and immunorecruitment phenotypes of microglia in the context of neuroinflammation.

Microglial NEDD4L Depletion Attenuates mtDNA-Mediated cGAS-Sting Activation Post-ICH

Among the multiple inflammatory pathways regulated by NEDD4L, the cytosolic DNA-sensing pathway particularly captured our interest(Figure 4A). While its role in the immune system is well-established, its specific functions in microglia following brain injury remain incompletely understood. We further explored the potential sources of DNA accumulated in cytosolic regulated by NEDD4L. Overexpression of NEDD4L in microglial cells led to a selective accumulation of mitochondrial DNA (mtDNA), but not nuclear DNA, within the cytosol(Figure 4B). Subsequent experiments involving pharmacological depletion of mtDNA using ethidium bromide over a three-week period completely abrogated the NEDD4L-induced production of proinflammatory cytokines, underscoring mtDNA release as a pivotal mechanism in driving NEDD4L mediated

inflammatory responses(Figure 4C-D).

Once released into the cytosol, mtDNA is recognized by specific pattern-recognition receptors involved in the DNA-sensing pathway, including cGAS, AIM2, and TLR9. These receptors initiate signaling cascades that promote inflammatory cytokines release(33). Our transcriptome data further indicated that NEDD4L modulates the expression of cGAS within this pathway(Figure 4E). Activation of cGAS by cytosolic mtDNA in turn stimulates the Sting-TBK1 signaling axis, leading to a type I interferon response. Immunoblot analyses confirmed that ICH induced upregulation of cGAS, Sting, and phosphorylation of TBK1(Figure 4F-I). Importantly, genetic ablation of NEDD4L in microglia markedly attenuated the activation of this cGAS-Sting-TBK1 pathway in mice subjected to ICH(Figure 4J-M). In summary, loss of NEDD4L in microglia restrains the leakage of mitochondrial DNA and thereby dampens the subsequent cGAS-Sting-dependent interferon response following ICH, highlighting a critical regulatory node in neuroinflammation.

NEDD4L Impairs Parkin-Dependent Mitophagy to Promote Cytosolic mtDNA Accumulation

Mitochondrial transcription factor A (TFAM) plays a critical role in preserving mtDNA integrity by facilitating structural stability and regulating replication(34). Although impaired TFAM function can induce mtDNA release, TFAM expression levels were not altered upon NEDD4L overexpression(Figure 5A-B). Another proposed route for mtDNA extrusion involves dysregulation of the mitochondrial permeability transition pore (mPTP)[35-38]; however, experimental modulation of NEDD4L did not affect mPTP activity(Figure 5C). Given these results, alternative pathways were investigated. Impaired mitophagy—a selective autophagic process responsible for clearing damaged

mitochondria—can lead to the accumulation of mtDNA in the cytosol[39]. In microglia, overexpression of NEDD4L was found to significantly disrupt mitophagy(Figure 5D-H). To identify NEDD4L-binding partners involved in mitophagy, we performed immunoprecipitation followed by mass spectrometry (IP–MS). HEK293T cells were transfected with a plasmid encoding NEDD4L or the corresponding empty vector control prior to analysis. Among the co-purified proteins, Parkin—a central mediator of mitophagic flux—was identified as a high-confidence interaction partner of NEDD4L(Figure 5I). Next, we performed cycloheximide (CHX) chase assays to evaluate the stability of Parkin proteins. In the cells transfected with the NEDD4L overexpress group, Parkin expression markedly decreased after treatment with CHX compared with the Vector group (Figure 5J -K). NEDD4L targets Parkin for its ubiquitination and degradation. In microglia, overexpression of NEDD4L significantly decrease Parkin protein level with LPS treatmen(Figure 5L-M). Physical interaction between NEDD4L and Parkin was confirmed via co-immunoprecipitation (Co-IP) in HEK293T cells expressing Flag-tagged NEDD4L and Myc-tagged Parkin(Figure 5N-O). Further analysis demonstrated that NEDD4L overexpression enhanced polyubiquitination of Parkin. Site-directed mutagenesis of ubiquitin lysine residues revealed that mutation at the K48 position abolished NEDD4L-induced polyubiquitination, indicating that NEDD4L promotes K48-linked polyubiquitination and subsequent proteasomal degradation of Parkin(Figure 5P). Moreover, NEDD4L was shown to regulate Parkin protein expression in primary microglia. Importantly, overexpression of Parkin reduced both cytosolic mtDNA levels (Figure 5Q-R)and the production of proinflammatory cytokines in this setting(Figure 5S-T). These findings indicated that NEDD4L interferes with Parkin-dependent mitophagy, resulting in pathological leakage of mitochondrial DNA into the cytosol and triggering the cGAS–Sting signaling axis.

Engineered EVs Delivering NEDD4L siRNA Attenuate Neuroinflammation After ICH via cGAS-Sting Axis

Next, we explored a targeted intervention strategy against NEDD4L with potential clinical applicability. In the absence of pharmacological inhibitors of NEDD4L, we aimed to silence NEDD4L expression using siRNA. To address the challenge of rapid siRNA degradation in vivo, we sought a suitable delivery vehicle and turned to extracellular vesicles (EVs), which have emerged as a promising cargo-delivery platform. EVs are lipid-membrane vesicles ranging from 30 to 150 nm in diameter, released by cells, capable of crossing the blood–brain barrier (BBB), and able to carry diverse molecular cargoes including proteins, lipids, and nucleic acids[40, 41]. To enhance microglia-specific targeting, we functionalized the EV surface with cRGD peptides (Arg-Gly-Asp-Phe-Val) using an incubation–extrusion-based lipid fusion technique[30]. This modification improves affinity for integrin αvβ3, which is highly expressed on hyperactivated microglia. We thus successfully generated engineered EVs loaded with NEDD4L siRNA and decorated with cRGD (referred to as cRGD-NEDD4Lsi-EVs). These vesicles were thoroughly characterized using transmission electron microscopy(Figure 6A) and nanoparticle tracking analysis for size distribution(Figure 6B) for morphological examination, and immunoblotting for EV-specific surface markers(Figure 6C-D). Biodistribution studies with DiI-labeled EVs revealed enhanced brain accumulation of cRGD-conjugated EVs 6 hours post-injection(Figure 6E-F). Immunofluorescence analysis confirmed their preferential uptake by microglia(Figure 6G). Moreover, qPCR analyses demonstrated significantly higher siRNA delivery efficiency with cRGD-NEDD4Lsi-EVs compared to cRGD-vector controls in ICH.(Figure 6H).

RNA sequencing identified 1175 significantly upregulated and 3602 downregulated

genes（Figure 6I）. Gene Ontology (GO) terms related to innate immune response and inflammatory pathways were markedly enriched（Figure 6J）. PCR results show microglial cell injection with cRGD-NEDD4Lsi-EVs can suppressed release of proinflammatory cytokines and chemokines (IL-1β, C3, IL-6, CCR5,CCR2 and CXC12)（Figure 6K）.

Therapeutic evaluations also showed that cRGD-NEDD4Lsi-EVs significantly reduced ICH-induced microglial activation (as indicated by $Iba1^{+}CD68^{+}$ cells)（Figure 6L-N）, IFNB1 mRNA level（Figure 6O）, TNF-α mRNA level（Figure 6P） and diminished peripheral immune cell infiltration（Figure 6Q-T）. Notably, Sting knockout in microglia ($Sting^{CKO}$ mice) attenuated neuroinflammatory responses compared to $Sting^{fl/fl}$ controls. Importantly, cRGD-NEDD4Lsi-EVs conferred no additional benefit in $Sting^{CKO}$ mice, indicating that their anti-inflammatory effects are dependent on the cGAS–Sting pathway.

7.Engineered EVs Delivering NEDD4L siRNA Attenuate Brain Injury after ICH and TBI via cGAS-Sting Axis

We next evaluated the therapeutic impact of cRGD-msiNEDD4L-EVs on secondary brain injury following ICH(Figure 7A). Volumetric analysis demonstrated diminished parenchymal damage in the treatment group(Figure 7B).Correspondingly, cerebral edema severity was markedly reduced following therapeutic administration(Figure 7C). Nissl staining further confirmed increased neuronal survival in in the treatment of cRGD-msiNEDD4L-EVs mice at 3 days after ICH (Figure 7D-E). TUNEL staining revealed significantly attenuated neuronal apoptosis in treated mice(Figure 7F-G). Behavioral

assessments—including adhesive removal(Figure 7H), grid-walking(Figure 7I), cylinder(Figure 7J) and rotarod tests(Figure 7K)—consistently indicated alleviated neurological deficits with cRGD-msiNEDD4L-EVs intervention. Notably, Sting-knockout mice exhibited intrinsically milder secondary injury compared to $Sting^{fl/fl}$ controls . Crucially, cRGD-msiNEDD4L-EVs administration failed to further mitigate pathology in $Sting^{CKO}$ mice. Collectively, these findings establish that engineered EVs-mediated siRNA NEDD4L delivery attenuates post-ICH secondary brain injury through cGAS-Sting pathway modulation. Furthermore, given our observation of specific NEDD4L upregulation in inflammatory microglia from TBI patients, we extended our therapeutic investigation to a TBI model using cRGD-msiNEDD4L-EVs intervention. This treatment yielded pronounced beneficial effects: it significantly reduced the TBI-induced ameliorated neuronal survival (Figure S3A-B), cerebral edema(Figure S3C) and improved neurological function(Figure S3D-G). Importantly, we confirmed that these therapeutic benefits were also dependent on the cGAS-Sting pathway, underscoring a conserved mechanism of action across different acute brain injury contexts.

Discussion

Acute brain injury triggers microglial hyperactivation and acute neuroinflammation, driving excessive cytokine production that exacerbates secondary injury. The molecular mechanisms governing microglial inflammatory responses remain poorly characterized. Our study reveals STAT2-mediated transcriptional activities significantly enhanced NEDD4L expression in post-ICH microglia. Critically, NEDD4L up-regulation promotes glial activation and neuroinflammatory cascades through impairing Parkin mediated mitophagy which lead to the activation of mtDNA-cGAS-Sting signaling. Engineered EVs delivering NEDD4L siRNA attenuate brain injury after ICH or TBI.These findings

establish NEDD4L as a key regulator of microglial pathophysiology with therapeutic implications.

NEDD4L, an E3 ubiquitin ligase, orchestrates diverse cellular functions via substrate-specific ubiquitination. Emerging evidence implicates NEDD4L in inflammation, neurodegeneration, and immunometabolism. This ubiquitin ligase exhibits context-dependent immunomodulation: it exacerbates neuroinflammation by promoting TRAF3/TBK1/NF-κB-mediated M1 macrophage polarization. Paradoxically, in Huntington's disease, NEDD4L upregulation induces mitochondrial dysfunction through LIPT2 ubiquitination, disrupting α-KGDH activity and oxidative phosphorylation while accelerating neuronal loss. Our investigation demonstrates significant NEDD4L upregulation in ICH or TBI-affected microglia. Genetic ablation attenuated glial inflammation and peripheral immune infiltration while improving edema, neuronal survival, and functional recovery. Transcriptomics confirmed NEDD4L's central role in microglial immune reprogramming post-ICH, highlighting its therapeutic potential.

The detection of exogenous DNA represents a cornerstone of innate immunity across species. In mammals, the cGAS- Sting signaling axis orchestrates this surveillance by inducing type I interferons and proinflammatory cytokines to mobilize host defenses. Notably, cGAS responds not only to microbial DNA but also to endogenous nucleic acids derived from nuclear or mitochondrial compartments. Beyond infectious contexts, this pathway participates in diverse physiological and pathological states—spanning antitumor immunity, cellular senescence, autophagy regulation, and inflammatory/autoimmune disorders. Emerging evidence implicates cGAS- Sting in neurological conditions including stroke, Parkinson's disease, traumatic brain injury, Alzheimer's dementia, and ALS, where its chronic activation exacerbates neuroinflammatory cascades. Our data reveal

pronounced cGAS- Sting activation following ICH, which is substantially attenuated by NEDD4L overexpression. Crucially, microglia-specific Sting ablation prevented ICH-induced neuroinflammation, while NEDD4L overexpression lost protective efficacy in Sting-deficient mice, establishing cGAS- Sting as the essential conduit for NEDD4L's anti-inflammatory actions.

Mechanistically, cytosolic mtDNA serves as the primary activator of cGAS- Sting signaling during ICH, a process fueled by mitochondrial dyshomeostasis. While mtDNA release can occur via TFAM depletion or permeability transition pore opening, we demonstrate that mitophagy impairment represents the dominant mechanism in ICH pathology. Supporting this, prior studies link defective mitophagy to mtDNA leakage and cGAS- Sting -driven inflammation, with microglial mitophagy deficiency documented post-stroke. Our work establishes that NEDD4L promotes cytosolic DNA accumulation via mitophagy disruption. Specifically, NEDD4L mediates K48-linked polyubiquitination and proteasomal degradation of Parkin—a key mitophagy regulator—in microglia, triggering mtDNA escape that activates cGAS- Sting and sustains pathological neuroinflammation.

To bridge our mechanistic findings with therapeutic potential, we investigated pharmacological interventions targeting NEDD4L. While genetic ablation effectively validated NEDD4L's role in ICH pathology, clinical translation necessitates non-invasive approaches. The blood-brain barrier (BBB) further constrains conventional drug delivery. To address this, we engineered cRGD-conjugated extracellular vesicles (cRGD-NEDD4Lsi-EVs) for brain-targeted siRNA delivery. In vivo studies demonstrated that intravenous cRGD-NEDD4Lsi-EVs significantly suppressed NEDD4L expression in microglia, attenuated neuroinflammation, and accelerated functional recovery. These data establish cRGD-EVs as a clinically viable platform for NEDD4L modulation in ICH.

Our study has several limitations warranting consideration. First, while collagenase-induced ICH models recapitulate key pathological features, they incompletely mimic human hematoma dynamics and comorbidities. Future investigations should incorporate aged models with hypertension and coagulopathy to enhance clinical relevance. Second, LPS-induced microglial polarization—though mechanistically informative—simplifies the continuum of in vivo activation states. Single-cell transcriptomics of ICH-affected microglia may reveal more nuanced NEDD4L regulatory networks. Finally, while cRGD-EVs show therapeutic promise, long-term biosafety and off-target effects require comprehensive evaluation in higher mammals prior to clinical translation.

In summary, NEDD4L emerges as a master regulator of neuroinflammation whose deficiency precipitates mtDNA-driven cGAS-Sting activation, sterile inflammation, and exacerbated brain injury. Therapeutic targeting of this pathway offers promising avenues for treating neuroimmune disorders of the CNS.

Figure Legend

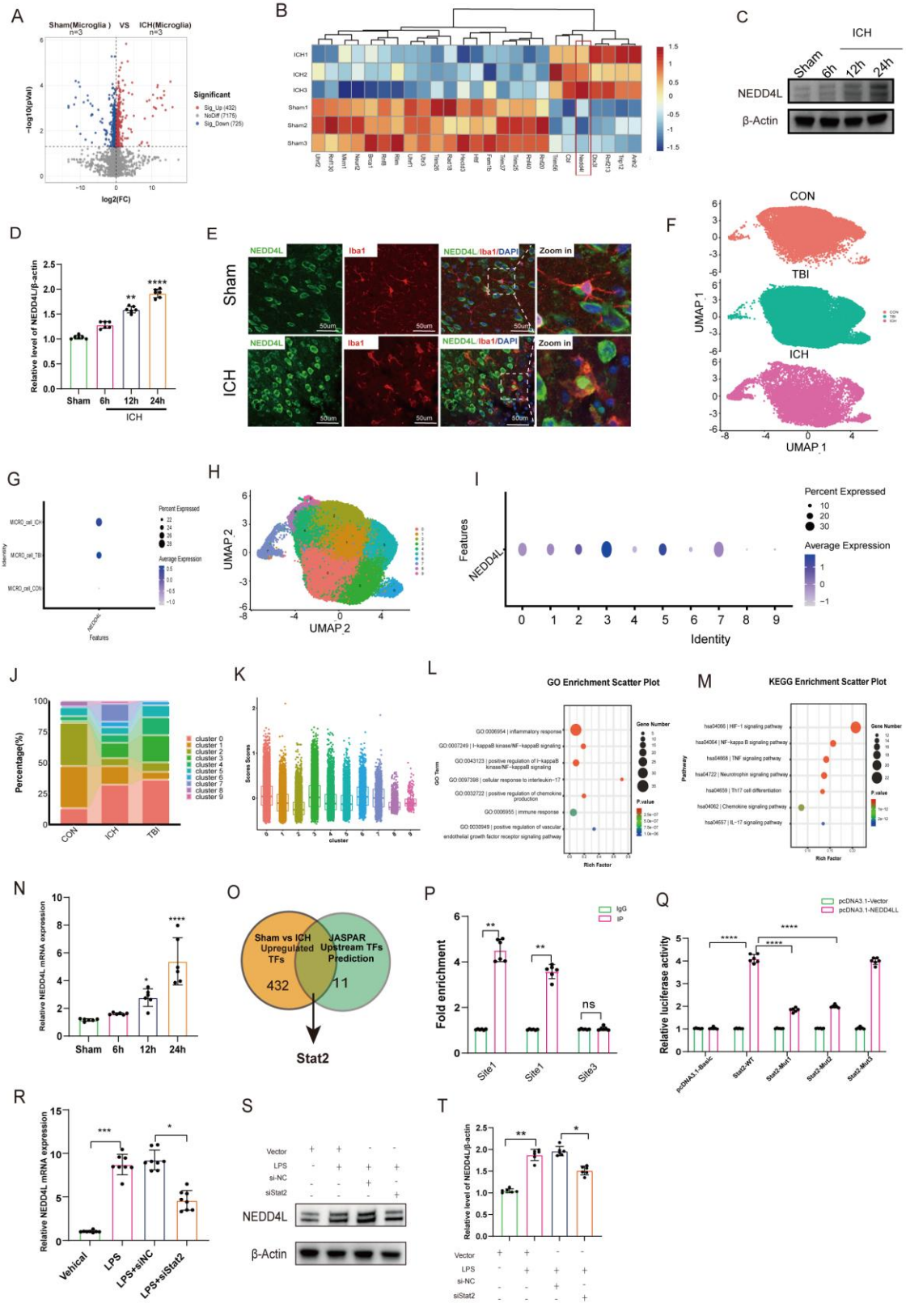

A
Sham(Microglia) VS ICH(Microglia)
n=3 n=3
Significant
Sig_Up (432)
NoDiff (7175)
Sig_Down (725)
−log10(pVal)
log2(FC)
B
C
ICH
Sham
6h
12h
24h
NEDD4L
β-Actin
D
Relative level of NEDD4L/β-actin
Sham
6h
12h
24h
ICH
E
NEDD4L
Iba1
NEDD4L Iba1/DAPI
Zoom in
Sham
ICH
50um
F
CON
TBI
ICH
UMAP_1
UMAP_2
G
Percent Expressed
Average Expression
Identity
Features
H
UMAP_2
I
Features
NEDD4L
Percent Expressed
Average Expression
Identity
J
Percentage(%)
CON
ICH
TBI
cluster 0
cluster 1
cluster 2
cluster 3
cluster 4
cluster 5
cluster 6
cluster 7
cluster 8
cluster 9
K
Scores
cluster
L
GO Enrichment Scatter Plot
GO:0006954 | inflammatory response
GO:0007249 | I-kappaB kinase/NF-kappaB signaling
GO:0043123 | positive regulation of I-kappaB kinase/NF-kappaB signaling
GO:0097398 | cellular response to interleukin-17
GO:0032722 | positive regulation of chemokine production
GO:0006955 | immune response
GO:0030949 | positive regulation of vascular endothelial growth factor receptor signaling pathway
GO Term
Gene Number
P.value
Rich Factor
M
KEGG Enrichment Scatter Plot
hsa04066 | HIF−1 signaling pathway
hsa04064 | NF−kappa B signaling pathway
hsa04668 | TNF signaling pathway
hsa04722 | Neurotrophin signaling pathway
hsa04659 | Th17 cell differentiation
hsa04062 | Chemokine signaling pathway
hsa04657 | IL−17 signaling pathway
Pathway
Gene Number
P.value
Rich Factor
N
Relative NEDD4L mRNA expression
Sham
6h
12h
24h
O
Sham vs ICH Upregulated TFs
432
JASPAR Upstream TFs Prediction
11
Stat2
P
IgG
IP
Fold enrichment
Site1
Site1
Site3
ns
Q
pcDNA3.1-Vector
pcDNA3.1-NEDD4LL
Relative luciferase activity
pcDNA3.1-Basic
Stat2-WT
Stat2-Mut1
Stat2-Mut2
Stat2-Mut3
R
Relative NEDD4L mRNA expression
Vehical
LPS
LPS+siNC
LPS+siStat2
S
Vector
LPS
si-NC
siStat2
NEDD4L
β-Actin
T
Relative level of NEDD4L/β-actin
Vector
LPS
si-NC
siStat2

Figure 1. Transcriptional upregulation of NEDD4L in inflammatory microglia by STAT2. (A) To identify microglial proteins altered after ICH, proteomic sequencing was performed on microglia isolated from ICH model mice. (B) Heatmap showing significantly dysregulated E3 ubiquitin ligases in post-ICH microglia. (C-D) Western blot quantification of NEDD4L protein levels in microglia after ICH (n=6/group; one-way ANOVA). (E) Immunofluorescence images co-staining NEDD4L (green) and the microglial marker Iba1 (red) in the ICH brain. (F) UMAP plot depicting microglia from human ICH, TBI, and control samples. (G) NEDD4L expression levels in these human microglial populations. (H) UMAP visualization of microglial subclusters (0-9). (I) NEDD4L expression across each subcluster. (J) Proportional distribution of microglial clusters among ICH, TBI, and control groups. (K) Pro-inflammatory gene module scores for each cluster, calculated using addModuleScore. (L-M) GO and KEGG pathway enrichment analyses for pro-inflammatory cluster 3. (N) qPCR analysis of NEDD4L mRNA in microglia sorted from ICH mice (n=6/group; one-way ANOVA). (O) Venn diagram identifying overlap between JASPAR-predicted transcription factors and those upregulated in proteomics. (P) ChIP-qPCR assay confirming Stat2 binding to the NEDD4L promoter region (n=6 wells/group). (Q) Luciferase reporter assay of the NEDD4L promoter with wild-type or deletion constructs, co-transfected with Stat2 (n=8 wells/group). (R-S) qPCR and Western blot analysis of NEDD4L expression after Stat2 knockdown in primary microglia (n=6/group). Data are mean ± SD. *P<0.05, **P<0.01, ***P<0.001.

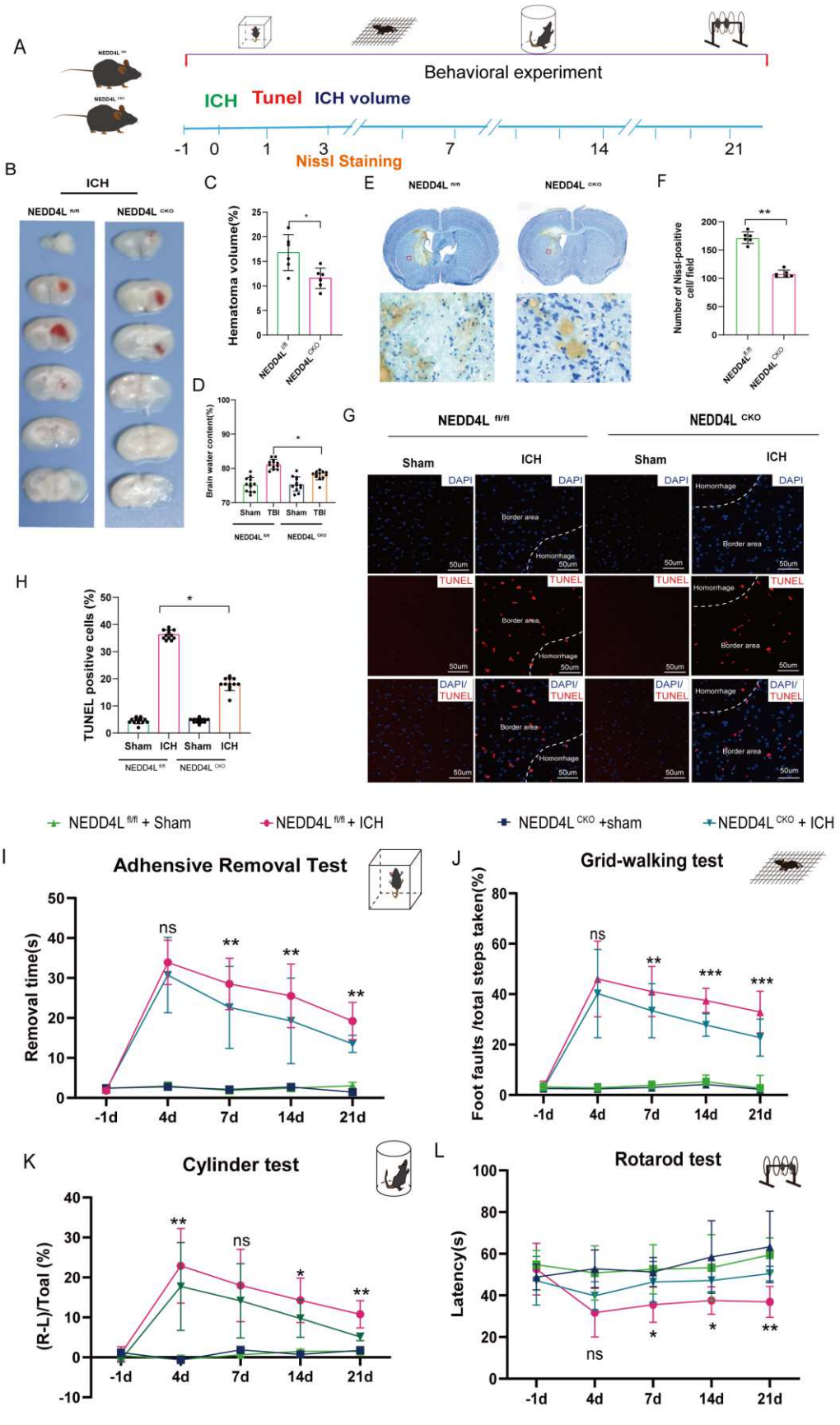

A
Behavioral experiment
ICH
Tunel
ICH volume
-1
0
1
3
7
14
21
Nissl Staining
B
ICH
NEDD4L fl/fl
NEDD4L CKO
C
Hematoma volume(%)
D
Brain water content(%)
Sham
TBI
E
F
Number of Nissl-positive cell/ field
G
Sham
ICH
DAPI
TUNEL
DAPI/ TUNEL
Homorrhage
Border area
50um
H
TUNEL positive cells (%)
NEDD4L fl/fl + Sham
NEDD4L fl/fl + ICH
NEDD4L CKO +sham
NEDD4L CKO + ICH
I
Adhensive Removal Test
Removal time(s)
ns
J
Grid-walking test
Foot faults /total steps taken(%)
K
Cylinder test
(R-L)/Toal (%)
L
Rotarod test
Latency(s)
-1d
4d
7d
14d
21d

Figure 2. Microglial NEDD4L knockout mitigates brain injury post-ICH. (A) Experimental timeline. (B–C) Hematoma volume at 3 d after ICH (n=6/group; Student's t-test). (D) Brain water content measurement (n=6/group; one-way ANOVA). (E–F) Surviving neurons visualized by Nissl staining at 3 d post-ICH (n=6/group; one-way ANOVA). (G–H) Representative TUNEL staining and quantification of apoptotic neurons (n=6/group; one-way ANOVA). (I–L) Sensorimotor function evaluated by adhesive removal (I), grid walking (J), cylinder (K), and rotarod (L) tests (n=12/group; two-way ANOVA). Data are mean ± SD. **P<0.01, ***P<0.001, ****P<0.0001.

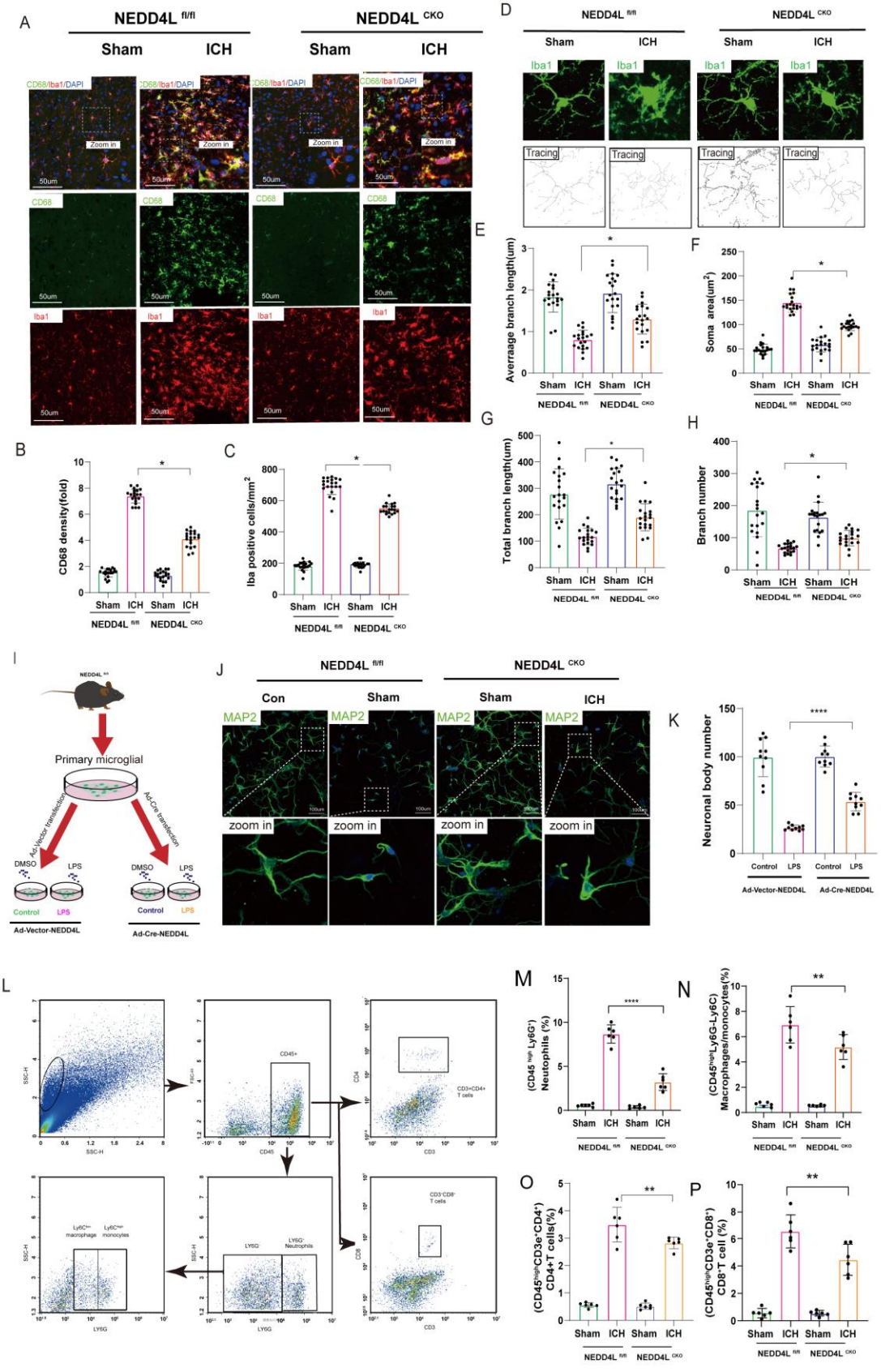

A
NEDD4L fl/fl
NEDD4L CKO
Sham
ICH
CD68/Iba1/DAPI
Zoom in
CD68
Iba1
50um
B
CD68 density(fold)
C
Iba positive cells/mm2
D
Tracing
E
Averrage branch length(um)
F
Soma area(um2)
G
Total branch length(um)
H
Branch number
I
Primary microglial
Ad-Vector transfection
Ad-Cre transfection
DMSO
LPS
Control
Ad-Vector-NEDD4L
Ad-Cre-NEDD4L
J
Con
MAP2
zoom in
K
Neuronal body number
L
CD45+
CD3+CD4+ T cells
CD3+CD8+ T cells
Ly6C++ macrophage
Ly6C++ monocytes
LY6G- Neutrophils
M
(CD45 high Ly6G+) Neutrophils (%)
N
(CD45highLy6G-Ly6C) Macrophages/monocytes(%)
O
(CD45highCD3e+CD4+) CD4+T cells(%)
P
(CD45highCD3e+CD8+) CD8+T cell (%)

Figure 3. NEDD4L deletion in microglia reduces neuroinflammation and neurotoxicity after ICH. (A) Representative immunofluorescence of Iba1 and CD68. (B–C) Quantification of Iba1$^+$cells and CD68 intensity 72 h post-ICH (n=20 slices from 6 mice/group; one-way ANOVA). (D) Example microglial images for morphology. (E–H) Skeleton-based morphometrics: soma area, branch number, total length (n=20 cells from 5 mice/group; one-way ANOVA). (I) Primary astrocytes from NEDD4L$^{fl/fl}$ mice infected with Ad-Vector or Ad-Cre. (J–K) MAP2$^+$ neuron soma size after treatment with conditioned medium from LPS-activated microglia with/without NEDD4L (n=6/group; one-way ANOVA). (L) Gating strategy for brain immune cell flow cytometry. (M–N) Quantification of Ly6G$^+$ neutrophils, Ly6G$^-$Ly6Clow macrophages, Ly6G$^-$Ly6Chigh monocytes, CD3$^+$CD4$^+$ and CD3$^+$CD8$^+$ T cells (n=6/group; Studen's t-test).Data are mean ± SD. **P<0.01, ***P<0.001, ****P<0.0001.

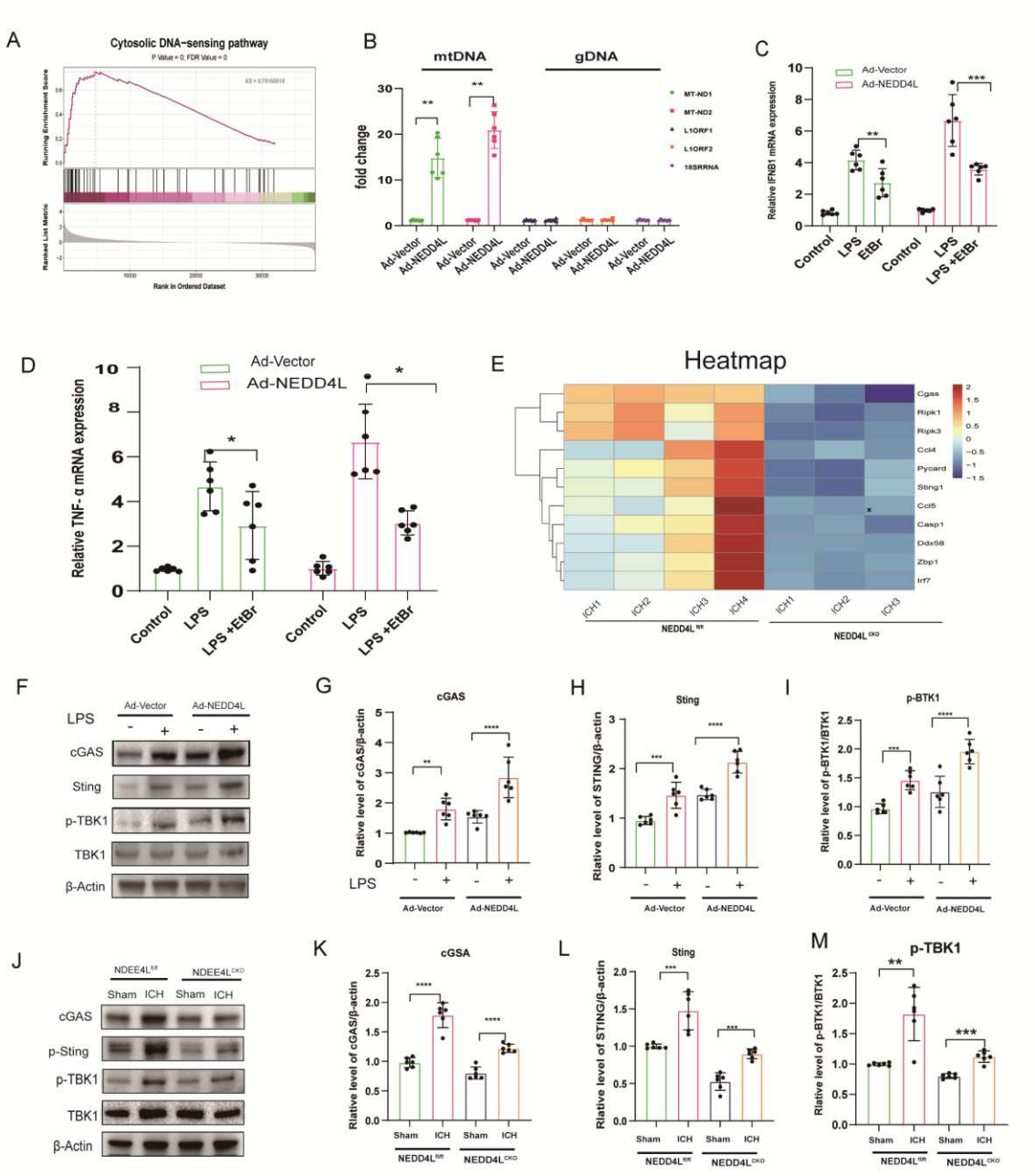
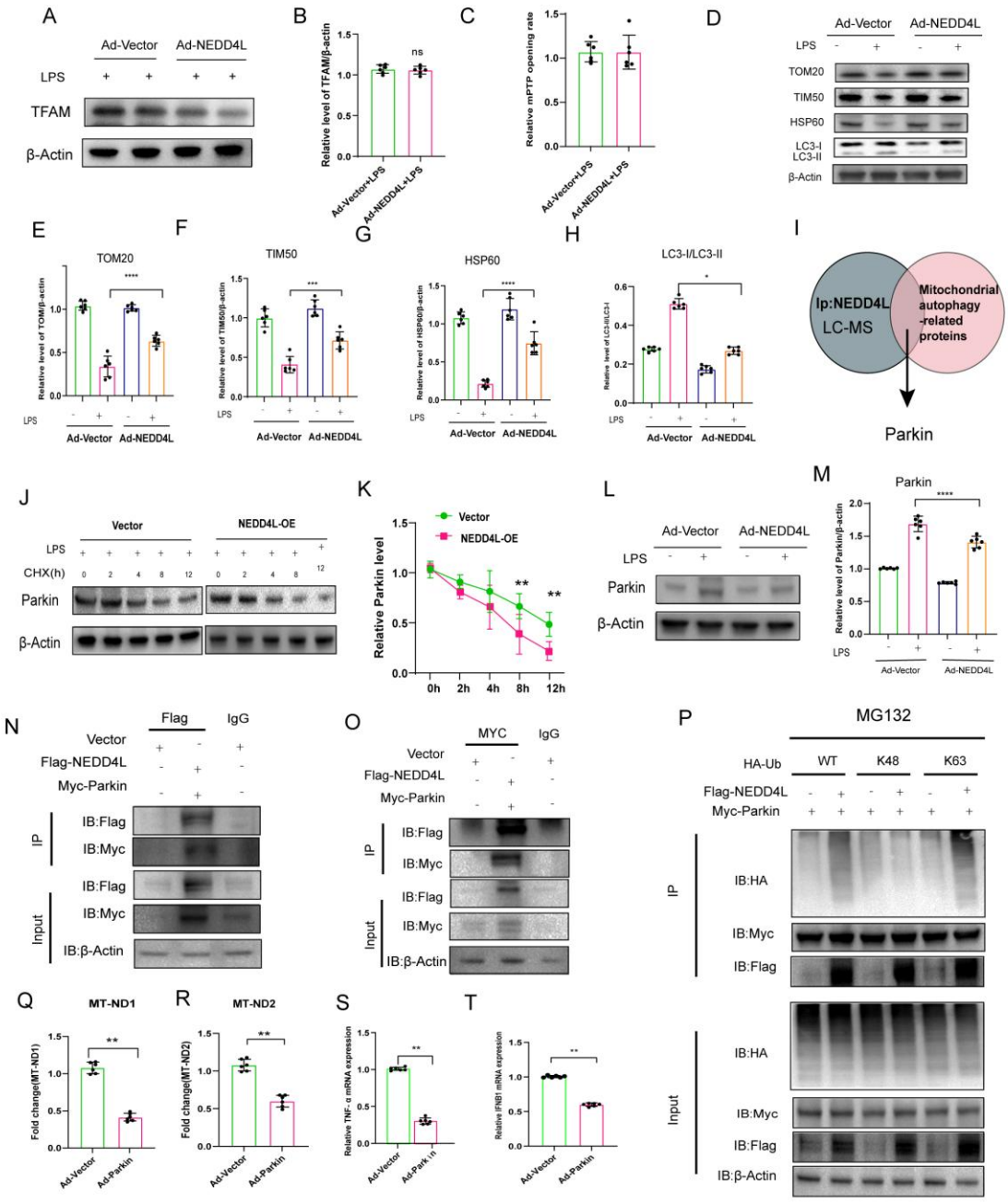


Figure 4. Microglial NEDD4L activates the cGAS－Sting pathway after ICH. (A) GSEA enrichment plot for the cytosolic DNA-sensing pathway among NEDD4L-regulated DEGs. (B) Cytosolic nuclear and mitochondrial DNA levels with/without NEDD4L overexpression (n=6/group; Student’s t-test). (C－D) IFNB1 and TNF expression in microglia treated with ethidium bromide (EtBr) to deplete mtDNA (n=6/group; two-way

ANOVA). (E) Heatmap of DEGs in the cytosolic DNA-sensing pathway. (F – G) Western blot of cGAS, Sting, TBK1, and p-TBK1 in primary microglia overexpressing NEDD4L (n=6/group; two-way ANOVA). (H – I) Western blot of these proteins in ICH mice with microglial NEDD4L knockout (n=6/group; two-way ANOVA). Data: mean ± SD. *P<0.05, **P<0.01, ***P<0.001.



1

2 **Figure 5. Microglial NEDD4L inhibits Parkin-mediated mitophagy, leading to**

3 **cytosolic mtDNA accumulation.** (A–B) Western blot of TFAM protein levels (two groups

4 shown; n=6/group; Student's t-test). (C) mPTP opening rate (n=6/group; Student's t-test).

(D–G) Western blot of TOM20, TIM50, LC3, and HSP60 in microglia treated with LPS or control (n=6/group; one-way ANOVA). (I) IP–MS in HEK293T cells transfected with NEDD4L or vector identified Parkin as an interactor. (J–K) Parkin protein levels in CHX-treated primary microglia with/without NEDD4L overexpression (n=6/group; two-way ANOVA). (L–M) Parkin levels in microglia transfected with Ad-Vector or Ad-NEDD4L and treated with LPS. (N–O) Co-IP in HEK293T cells expressing Myc-Parkin and Flag-NEDD4L. (P) Ubiquitination assay in cells co-expressing Myc-Parkin, Flag-NEDD4L, and HA-Ub (WT, K48, K63); IP with anti-Myc, blot with anti-HA/Flag. (Q–R) Effect of Parkin overexpression on NEDD4L-induced mtDNA leakage (n=6/group; one-way ANOVA). (S–T) Effect of Parkin overexpression on NEDD4L-induced IFNB1 and TNF expression (n=6/group; one-way ANOVA). Data: mean ± SD. *P<0.05, **P<0.01, ***P<0.001.

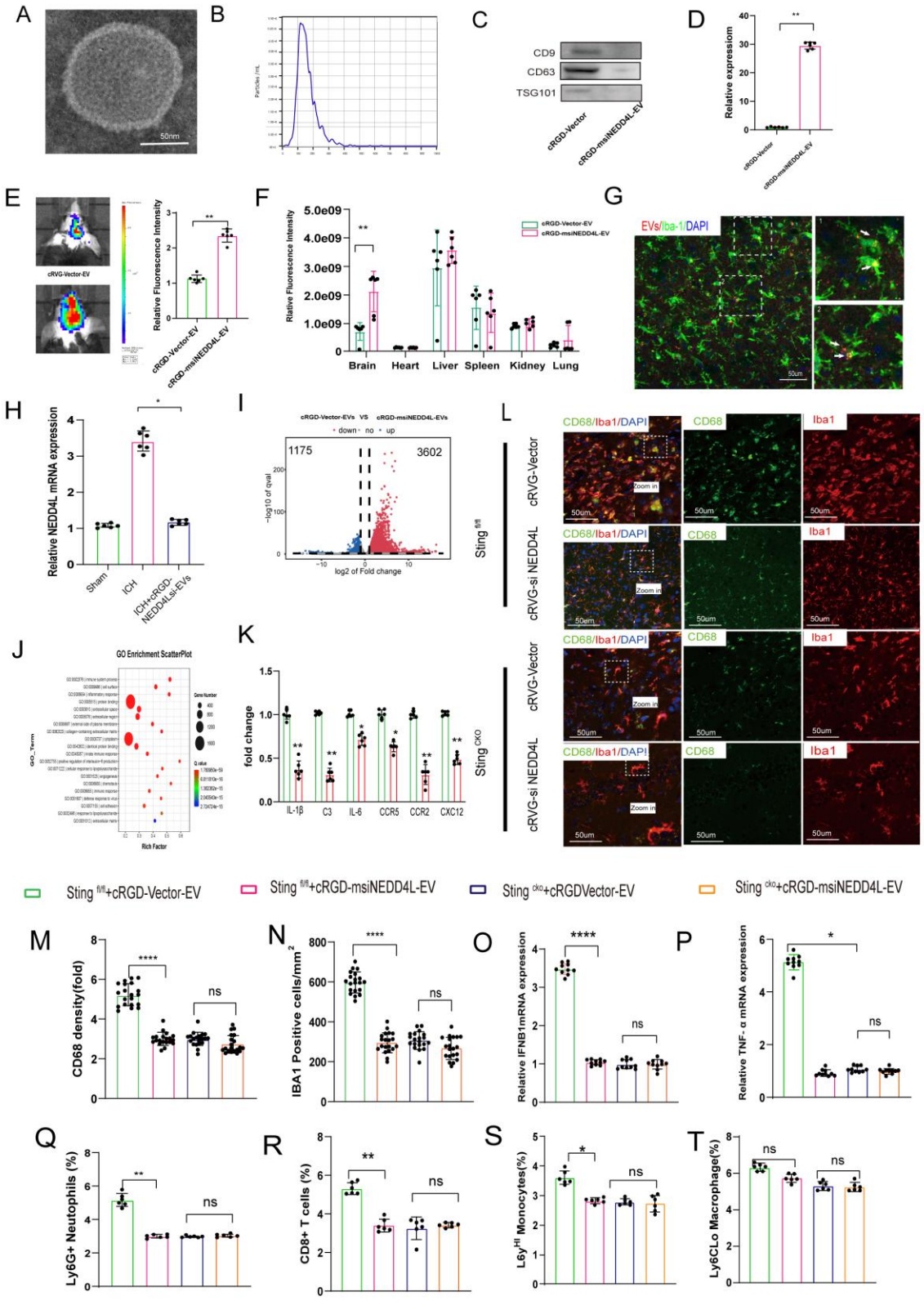

A
50nm
B
C
CD9
CD63
TSG101
cRGD-Vector
cRGD-msiNEDD4L-EV
D
Relative expression
E
cRVG-Vector-EV
Relative Fluorescence Intensity
F
Rlative Fluorescence Intensity
cRGD-Vector-EV
cRGD-msiNEDD4L-EV
Brain
Heart
Liver
Spleen
Kidney
Lung
G
EVs/Iba-1/DAPI
H
Relative NEDD4L mRNA expression
Sham
ICH
ICH+cRGD-NEDD4LsiRNA-EVs
I
cRGD-Vector-EVs VS cRGD-msiNEDD4L-EVs
down no up
1175
3602
log2 of Fold change
Sting fl/fl
L
CD68/Iba1/DAPI
CD68
Iba1
cRVG-Vector
cRVG-si NEDD4L
Zoom in
50um
J
GO Enrichment ScatterPlot
Rich Factor
K
fold change
IL-1β
C3
IL-6
CCR5
CCR2
CXC12
Sting CKO
Sting fl/fl+cRGD-Vector-EV
Sting fl/fl+cRGD-msiNEDD4L-EV
Sting cko+cRGDVector-EV
Sting cko+cRGD-msiNEDD4L-EV
M
CD68 density(fold)
N
IBA1 Positive cells/mm2
O
Relative IFNB1mRNA expression
P
Relative TNF- α mRNA expression
Q
Ly6G+ Neutophils (%)
R
CD8+ T cells (%)
S
Ly6CHI Monocytes(%)
T
Ly6CLo Macrophage(%)
ns

Figure 6. cRGD-engineered EVs delivering NEDD4L siRNA alleviate neuroinflammation via cGAS–STING. (A) TEM image of uranyl acetate-stained cRGD-EVs. (B) NTA size distribution of cRGD-EVs. (C–D) Western blot of EV markers (n=6/group; one-way ANOVA). (E–F) Biodistribution of DiR-labeled nontargeting EVs vs. cRGD-EVs in ICH mice 24 h post-injection (n=6/group; Student's t-test). (G) Immunofluorescence showing EV uptake by microglia 24 h post-injection. (H) cRGD-msiNEDD4L-EVs reduced NEDD4L expression in the ICH lesion. (I) Volcano plot of DEGs in microglia from ICH vs. Sham mice. (J) GO analysis of DEGs after cRGD-msiNEDD4L-EV treatment. (K) qPCR of IL-1β, C3, IL-6, CCR5, CCR2, and CXCL12 (n=6/group; one-way ANOVA). (L) Representative Iba1 and CD68 co-staining. (M–N) Quantification of $Iba1^+$ cells and CD68 intensity 72 h post-ICH (n=18 slices from 6 mice/group; one-way ANOVA). (O–P) Flow cytometry counts of neutrophils, macrophages/monocytes, $CD4^+$, and $CD8^+$ T cells (n=6/group; one-way ANOVA). (Q–R) Effects of cRGD-msiNEDD4L-EVs on IFNB1 and TNF-α in $Sting^{fl/fl}$ and $Sting^{CKO}$ mice (n=6/group; one-way ANOVA). Data: mean ± SD. *P<0.05, **P<0.01, ***P<0.001.

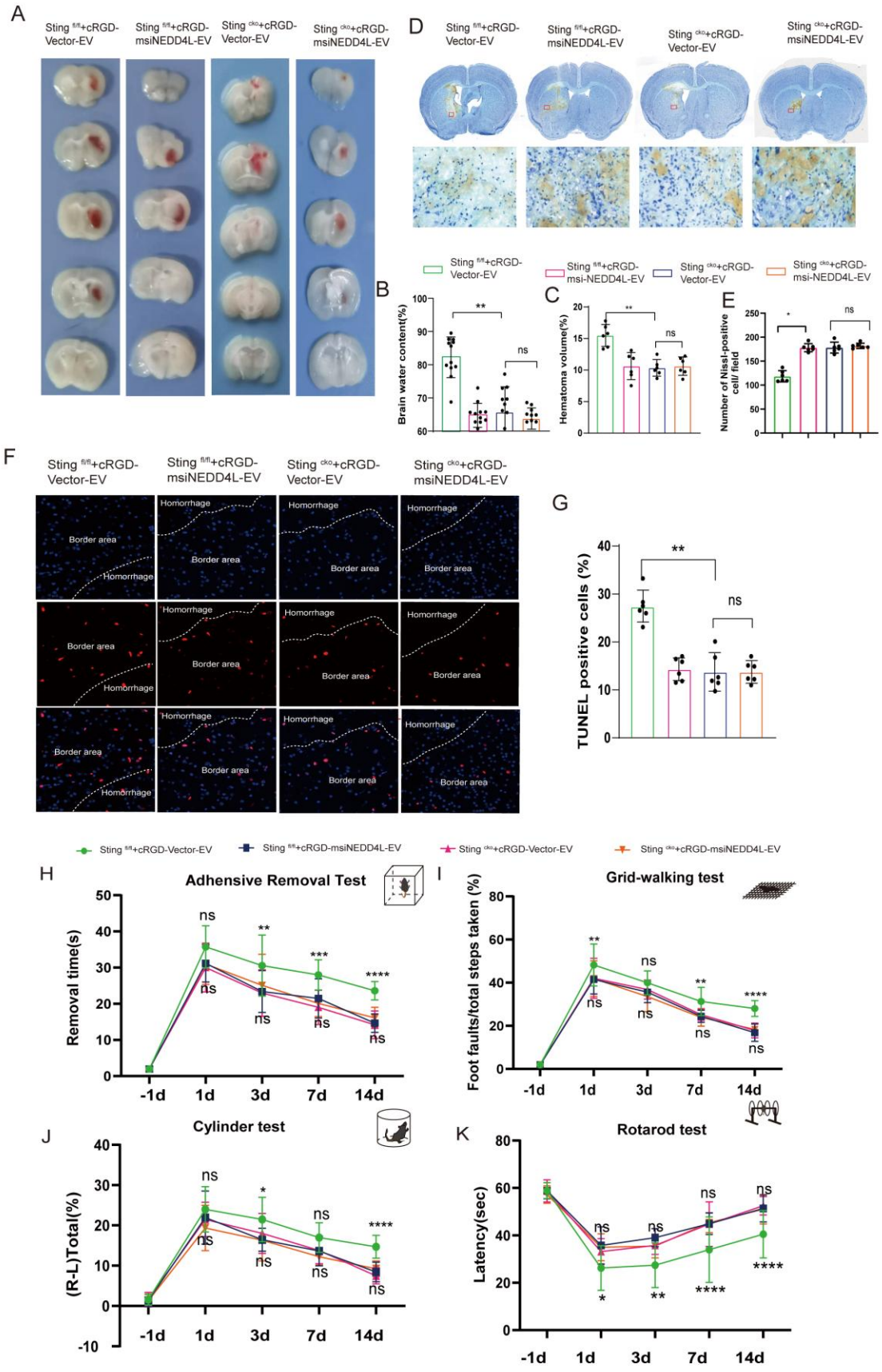

A
Sting fl/fl+cRGD-Vector-EV
Sting fl/fl+cRGD-msiNEDD4L-EV
Sting cko+cRGD-Vector-EV
Sting cko+cRGD-msiNEDD4L-EV
D
B
Brain water content(%)
C
Hematoma volume(%)
E
Number of Nissl-positive cell/ field
Sting fl/fl+cRGD-msi-NEDD4L-EV
Sting cko+cRGD-msi-NEDD4L-EV
F
Homorrhage
Border area
G
TUNEL positive cells (%)
H
Adhensive Removal Test
Removal time(s)
I
Grid-walking test
Foot faults/total steps taken (%)
J
Cylinder test
(R-L)Total(%)
K
Rotarod test
Latency(sec)
-1d
1d
3d
7d
14d
ns

Figure 7. cRGD-NEDD4Lsi-EV treatment reduces ICH injury via cGAS–STING. (A–B) Representative images and quantification of hematoma volume 3 d post-ICH (n=6/group; Student's t-test). (C) Brain water content (n=6/group; one-way ANOVA). (D–E) Nissl-stained sections and TUNEL-based apoptosis quantification (n=6/group; Student's t-test). (F–I) Sensorimotor tests: adhesive removal (F), grid walking (G), cylinder (H), rotarod (I) (n=12/group; two-way ANOVA). Data: mean ± SD. *P<0.05, **P<0.01, ***P<0.001.

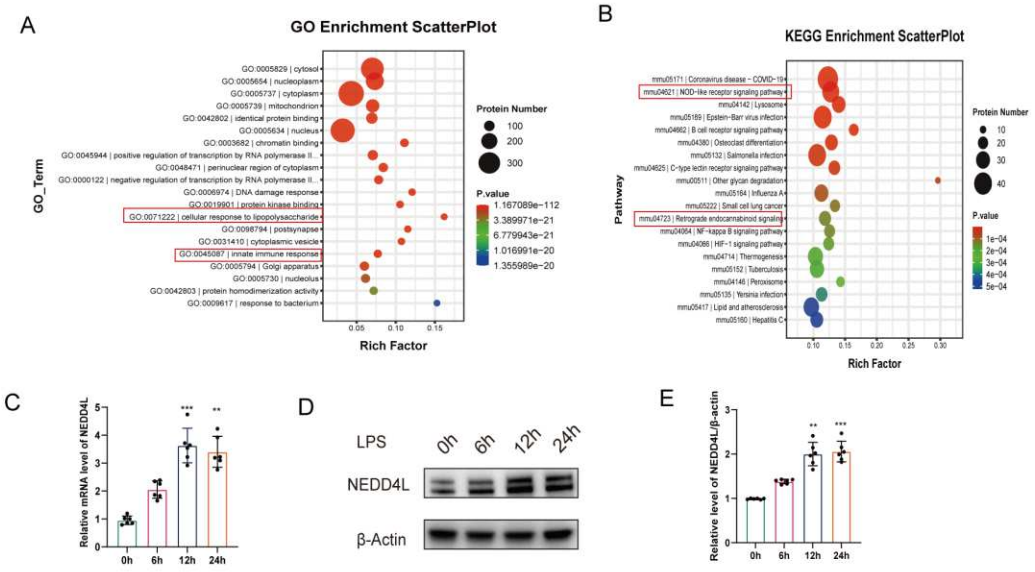


Figure S1. Elevated NEDD4L expression in activated microglia. (A-B) GO and KEGG enrichment analyses of differentially expressed proteins in microglia following ICH. (C) qPCR analysis of NEDD4L mRNA in primary microglia stimulated with LPS (n=6/group; one-way ANOVA). (D-E) Western blot and quantification of NEDD4L protein in LPS-

treated primary microglia (n=6/group; one-way ANOVA). Data are mean ± SD. **P<0.01, ***P<0.001, ****P<0.0001.

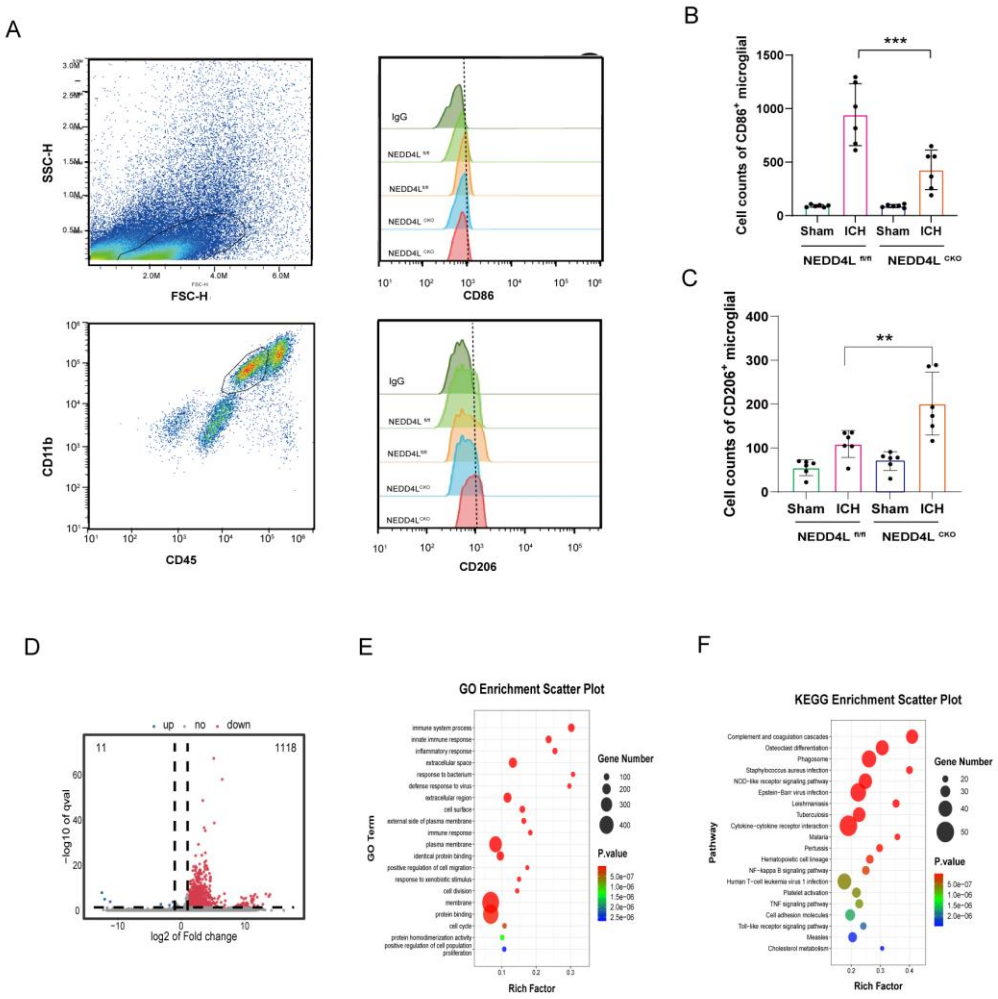


Figure S2. NEDD4L knockout attenuates neuroinflammatory responses. (A – C) Flow cytometry analysis of M1/M2 microglial polarization ratios. (D) Volcano plot of differentially expressed genes (DEGs) in microglia from ICH vs. Sham mice. (E – F) GO and KEGG pathway analysis of DEGs.

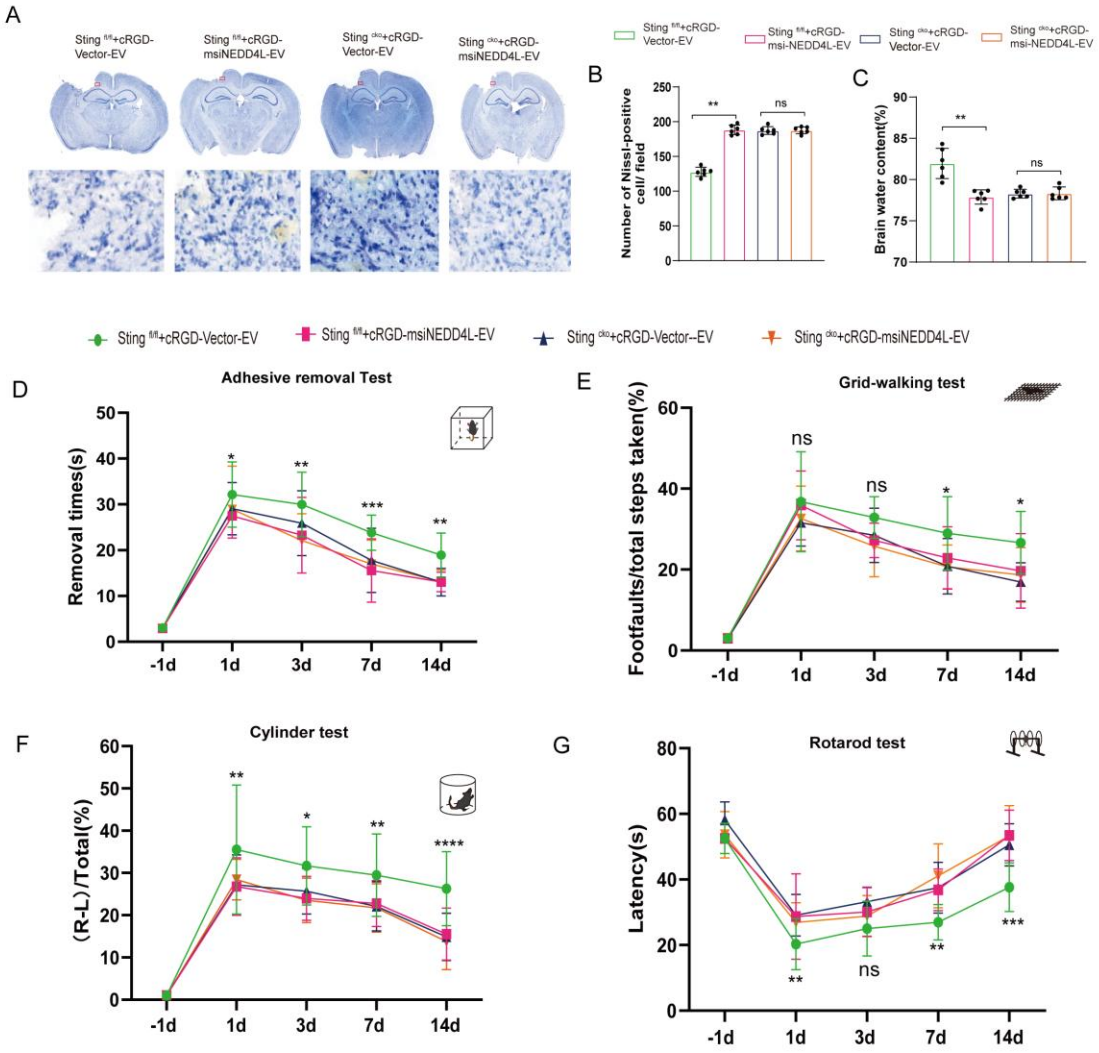


Figure S3 cRGD-NEDD4Lsi-EV injection attenuated brain injury after TBI in a cGAS-Sting-dependent manner. (A-B) Nissl- stained brain sections after ICH (n=6 per group, one-way ANOVA) (C) Measurement of brain water content (n=6 per group, one-way ANOVA). (D-G) Assessment of sensorimotor function using the adhesive removal test (D), grid walking test (E), cylinder test (F), and rotarod test (G) (n=15 per group, two-way ANOVA). Data are presented as means ± SD. *P < 0.05, **P < 0.01, ***P < 0.001, ****P

< 0.001.

Declarations

Ethical Approval and Consent to participate

All animal and human tissue studies were approved by Ethics Committee of Zhejiang Provincial People's Hospital. Written informed consent for publication was obtained from the patient.

Consent for publication

Written informed consent for publication of this paper was obtained from all authors.

Availability of data and materials

Not applicable.

Competing interest

All authors declare that they have no conflict of interest.

Funding

This study was funded by Zhejiang Provincial Natural Science Foundation of China (No. LTGY23H090016) and Gansu Youth Science and Technology Fund（24JRRA009）.

Author contributions

Authors' contributions: J.W.,WH.Z. and SH.Z contributed to figures preparation. YH.Z., WY.W. SL.W.,X.G., SC.F. performed additional in vitro and in vivo experiments. J.W. and YY.M. wrote the manuscript. KC.Y.and X.W. designed and supervised the study. B.L. edited the manuscript.

Acknowledgments

We appreciate home for researchers (www.home- for- researchers.com) for language editing and scheme optimization. We also appreciate Shaoshan Hu MD, PhD, Zhejiang Provincial People's Hospital, Hangzhou Medical College for technical guidance.

References

1. Wu X, Liu H, Wang J, Zhang S, Hu Q, Wang T, et al. The m(6)A methyltransferase METTL3 drives neuroinflammation and neurotoxicity through stabilizing BATF mRNA in microglia. Cell death and differentiation. 2025;32(1):100-17.
2. Lawrence AR, Canzi A, Bridlance C, Olivié N, Lansonneur C, Catale C, et al. Microglia maintain structural integrity during fetal brain morphogenesis. Cell. 2024;187(4):962-80.e19.
3. Faust TE, Lee YH, O'Connor CD, Boyle MA, Gunner G, Durán-Laforet V, et al. Microglia-astrocyte crosstalk regulates synapse remodeling via Wnt signaling. Cell. 2025;188(19):5212-30.e21.
4. Wang L, Ouyang D, Li L, Cao Y, Wang Y, Gu N, et al. TREM2 affects DAM-like cell transformation in the acute phase of TBI in mice by regulating microglial glycolysis. Journal of neuroinflammation. 2025;22(1):6.
5. Zhang H, Zhong Y, Shao J, Sun K, Zhang L, Zhang Y, et al. Influx of Metabolites into Cerebrospinal Fluid in Intracerebral Hemorrhage is Associated with Increased Central Inflammation: a Retrospective Observational Study. Translational stroke research. 2025;16(5):1710-22.
6. Wu JW, Zhou YT, Wang BX, Wang P, Zhang XQ, Du SQ, et al. Network Pharmacology-Based and Experimental Validation Elucidate the Target Mechanism of Vinorine in Ameliorating Secondary Brain Injury After Intracerebral Hemorrhage. CNS neuroscience & therapeutics. 2025;31(9):e70609.
7. Placeres-Uray F, Gorthy AS, Torres MD, Atkins CM. Inhibition of microglia priming by NLRP3 reduces the impact of early life stress and mild TBI. Journal of neuroinflammation. 2025;22(1):185.
8. Wan H, He M, Cheng C, Yang K, Wu H, Cong P, et al. Clec7a Worsens Long-Term Outcomes after Ischemic Stroke by Aggravating Microglia-Mediated Synapse Elimination. Advanced science (Weinheim, Baden-Wurttemberg, Germany). 2024;11(36):e2403064.
9. Lee E, Hwang I, Park S, Hong S, Hwang B, Cho Y, et al. MPTP-driven NLRP3 inflammasome activation in microglia plays a central role in dopaminergic neurodegeneration. Cell death and differentiation. 2019;26(2):213-28.
10. Zhao L, Li T, Dang M, Li Y, Lu J, Lu Z, et al. Succinate Dehydrogenase Subunit A (SDHA) Mediated Microglia Extracellular Traps Formation Participating in Cerebral Ischemic Reperfusion Injury. Advanced science (Weinheim,

Baden-Wurttemberg, Germany). 2025;12(35):e11873.
11. Manning JA, Shah SS, Nikolic A, Henshall TL, Khew-Goodall Y, Kumar S. The ubiquitin ligase NEDD4-2/NEDD4L regulates both sodium homeostasis and fibrotic signaling to prevent end-stage renal disease. Cell death & disease. 2021;12(4):398.
12. Fan P, Liu Y, Liu C, Yao H, Xu S, Jiang Y, et al. NEDD4L induces mitochondrial dysfunction and neurodegeneration by promoting LIPT2 degradation in Huntington's disease. Proceedings of the National Academy of Sciences of the United States of America. 2025;122(29):e2503342122.
13. Han F, Wu S, Dong Y, Liu Y, Sun B, Chen L. Aberrant expression of NEDD4L disrupts mitochondrial homeostasis by downregulating CaMKKβ in diabetic kidney disease. Journal of translational medicine. 2024;22(1):465.
14. Gao P, Ma X, Yuan M, Yi Y, Liu G, Wen M, et al. E3 ligase NEDD4L promotes antiviral innate immunity by catalyzing K29-linked cysteine ubiquitination of TRAF3. Nature communications. 2021;12(1):1194.
15. Peng M, Zhao C, Lu F, Zhang X, Wang X, He L, et al. Role of NEDD4L in Macrophage Pro-Inflammatory Polarization Induced by Influenza A Virus and Lipopolysaccharide Stimulation. Microorganisms. 2024;12(7).
16. Liu Q, Ling Z, Zhang J, Yu H, Wang Y, Xue Y, et al. lncRNA MIR600HG Knockdown Alleviates Cognitive Impairment in Alzheimer's Disease Through NEDD4L Mediated PINK1 Degradation. Journal of Alzheimer's disease : JAD. 2022;85(4):1783-94.
17. He S, Pan T, Tian R, He Q, Cheng D, Qu H, et al. Fatty acid synthesis promotes mtDNA release via ETS1-mediated oligomerization of VDAC1 facilitating endothelial dysfunction in sepsis-induced lung injury. Cell death and differentiation. 2025.
18. Hu X, Zhang H, Zhang Q, Yao X, Ni W, Zhou K. Emerging role of STING signalling in CNS injury: inflammation, autophagy, necroptosis, ferroptosis and pyroptosis. Journal of neuroinflammation. 2022;19(1):242.
19. Guey B, Wischnewski M, Decout A, Makasheva K, Kaynak M, Sakar MS, et al. BAF restricts cGAS on nuclear DNA to prevent innate immune activation. Science (New York, NY). 2020;369(6505):823-8.
20. Li RF, Liu S, Gao Q, Fu M, Sun XY, Xiao M, et al. Inhibition of CDH11 Activates cGAS-STING by Stimulating Branched Chain Amino Acid Catabolism and Mitigates Lung Metastasis of Adenoid Cystic Carcinoma. Advanced science (Weinheim, Baden-Wurttemberg, Germany). 2025;12(8):e2408751.
21. Xue Q, Lai H, Zhang H, Li G, Pi F, Wu Q, et al. Selenium Attenuates Radiation Colitis by Regulating cGAS-STING Signaling. Advanced science (Weinheim, Baden-Wurttemberg, Germany). 2024;11(44):e2403918.
22. Ma D, Yang M, Sun C, Cui X, Xiong G, Wang Q, et al. cGAS suppresses hepatocellular carcinoma independent of its cGAMP synthase activity. Cell death and differentiation. 2024;31(6):722-37.
23. Li H, Cai R, Zhou Y, Jiang Y, Tan S. cGAS-STING signaling in brain aging and neurodegeneration: molecular links and therapeutic perspectives. Journal of neuroinflammation. 2025;22(1):235.
24. Zhang G, Wei H, Zhao A, Yan X, Zhang X, Gan J, et al. Mitochondrial DNA leakage: underlying mechanisms and therapeutic implications in neurological disorders. Journal of neuroinflammation. 2025;22(1):34.
25. Huang Y, Liu B, Sinha SC, Amin S, Gan L. Mechanism and therapeutic potential of targeting cGAS-STING signaling in neurological disorders. Molecular neurodegeneration. 2023;18(1):79.
26. Zhang W, Xu M, Chen F, Su Y, Yu M, Xing L, et al. Targeting the JAK2-STAT3 pathway to inhibit cGAS-STING activation improves neuronal senescence after ischemic stroke. Experimental neurology. 2023;368:114474.
27. Wu X, Cui W, Guo W, Liu H, Luo J, Zhao L, et al. Acrolein Aggravates Secondary Brain Injury After Intracerebral Hemorrhage Through Drp1-Mediated Mitochondrial Oxidative Damage in Mice. Neuroscience bulletin.

2020;36(10):1158-70.
28. Luo J, Wu X, Liu H, Cui W, Guo W, Guo K, et al. Antagonism of Protease-Activated Receptor 4 Protects Against Traumatic Brain Injury by Suppressing Neuroinflammation via Inhibition of Tab2/NF-κB Signaling. Neuroscience bulletin. 2021;37(2):242-54.
29. Gosselin D, Skola D, Coufal NG, Holtman IR, Schlachetzki JCM, Sajti E, et al. An environment-dependent transcriptional network specifies human microglia identity. Science (New York, NY). 2017;356(6344).
30. Liu Y, Xia P, Yan F, Yuan M, Yuan H, Du Y, et al. Engineered Extracellular Vesicles for Delivery of an IL-1 Receptor Antagonist Promote Targeted Repair of Retinal Degeneration. Small (Weinheim an der Bergstrasse, Germany). 2023;19(46):e2302962.
31. Wu X, Liu H, Hu Q, Wang J, Zhang S, Cui W, et al. Astrocyte-Derived Extracellular Vesicular miR-143-3p Dampens Autophagic Degradation of Endothelial Adhesion Molecules and Promotes Neutrophil Transendothelial Migration after Acute Brain Injury. Advanced science (Weinheim, Baden-Wurttemberg, Germany). 2024;11(5):e2305339.
32. Zhou J, Ma S, Feng D, Tian Y, Li L, Guo H, et al. C5aR1(+) microglia exacerbate neuroinflammation and cerebral edema in acute brain injury. Neuron. 2025.
33. Xiang M, Yang M, Zhang L, Ouyang X, Sarapultsev A, Luo S, et al. Mitochondrial DNA Dysfunction in Cardiovascular Diseases: A Novel Therapeutic Target. Antioxidants (Basel, Switzerland). 2025;14(9).
34. Li Y, Yang Q, Chen H, Yang X, Han J, Yao X, et al. TFAM downregulation promotes autophagy and ESCC survival through mtDNA stress-mediated STING pathway. Oncogene. 2022;41(30):3735-46.
35. Yang Y, Zeng Y, Zhu J, Li J, Gu L, Wei L, et al. OMP38 of Carbapenem-Resistant Acinetobacter Baumannii-Mediated mtDNA Release Activates the cGAS-STING Signaling to Induce Inflammatory Response. Advanced science (Weinheim, Baden-Wurttemberg, Germany). 2024;12(4):e2408292.
36. Xiong Y, Chen J, Liang W, Li K, Huang Y, Song J, et al. Blockade of the mitochondrial DNA release ameliorates hepatic ischemia-reperfusion injury through avoiding the activation of cGAS-Sting pathway. Journal of translational medicine. 2024;22(1):796.
37. Li Y, Cui J, Liu L, Hambright WS, Gan Y, Zhang Y, et al. mtDNA release promotes cGAS-STING activation and accelerated aging of postmitotic muscle cells. Cell death & disease. 2024;15(7):523.
38. Liu Z, Wang M, Wang X, Bu Q, Wang Q, Su W, et al. XBP1 deficiency promotes hepatocyte pyroptosis by impairing mitophagy to activate mtDNA-cGAS-STING signaling in macrophages during acute liver injury. Redox biology. 2022;52:102305.
39. Lu Y, Gao L, Yang Y, Shi D, Zhang Z, Wang X, et al. Protective role of mitophagy on microglia-mediated neuroinflammatory injury through mtDNA-STING signaling in manganese-induced parkinsonism. Journal of neuroinflammation. 2025;22(1):55.
40. Guo S, Wang Z, Shi R, Huang P, Fang Y, Chen S, et al. Engineered extracellular vesicles for targeted FGF20 delivery enhance neuroplasticity and functional recovery in ischemic stroke. Journal of controlled release : official journal of the Controlled Release Society. 2025;386:114080.
41. Li T, Wang P, Li F, Chen K, Yu J, Ma C, et al. Engineered neural stem cell vesicles activating Wnt promote blood-brain barrier repair after cerebral haemorrhage. Brain : a journal of neurology. 2025.